DÉPARTEMENT DE GÉNIE MÉCANIQUE
SECTION MÉCANIQUE APPLIQUÉE

VOID FRACTION IN HIGHLY TURBULENT AND LARGE DIAMETER HORIZONTAL PIPE FLOW

by

Aouni A. LAKIS and Nguyen D. TRINH

September 1988 No. EPM/RT-88-28

VOID FRACTION IN HIGHLY TURBULENT

AND

LARGE DIAMETER HORIZONTAL PIPE FLOW

by

Aouni A. LAKIS and Nguyen D. TRINH

Technical Report
No. EPM/RT-88-
1988

Department of Mechanical Engineering
Ecole Polytechnique de Montréal
University of Montreal
P.O. Box 6079, Station A, Montreal
Quebec, Canada, H3C 3A7

TABLE OF CONTENTS

VOID FRACTION IN HIGHLY TURBULENT AND LARGE DIAMETER HORIZONTAL PIPE FLOW

ABSTRACT

This study presents an experimental prediction of void fraction distribution in large diameter horizontal pipe flow. A turbulent air-water mixture flows through a series of 8-in. diameter pipes, with a Reynolds number of 2.10^6 on a liquid basis and a 30% maximum flow volumetric quality under normal operating conditions. A double conical hot film has been designed to simultaneously measure the void fraction and bubble velocity. The hot film probe was calibrated in a 2-in. diameter bubbly pipe flow. Measured local void fractions were corrected by the quick closing valves global method through an improved calibration procedure. Tests were carried out along the pipe axis and in both cross-sectional planes. Fully-developped flow was identified at a distance more than 100 times pipe diameter from the mixer. Non-uniformity of the profiles revised only in the transversal plane. Void measurements in the horizontal large diameter pipe were found to be qualitatively comparable with numerical results in 1.0-in. diameter horizontal pipe (Brown and Kranich [9]). Two new sets of correlations are proposed here. The first predicts the longitudinal distribution of void fraction, where correlations are expressed in terms of axial location and flow volumetric quality. In the second, distribution

of void fraction in transversal plane may be predicted either by the linear - or exponential model. Void fraction profiles were found to be almost flat in the radial plane and for which the power law may be assumed.

REMERCIEMENTS

Ce document a pu être publié grâce à une subvention du Conseil de recherches en sciences et en génie du Canada (CRSNG) (Subv: no. A-8814) et le F.C.A.R. du Québec (Subv: no. CRP-2060).

Nous tenons à remercier Mme Guylaine Dagenais qui a dactylographié tous nos textes, modèles et formulaire.

Dépôt légal, 2e trimestre 1986
Bibliothèque nationale du Québec
Bibliothèque nationale du Canada

Pour se procurer une copie de ce document, s'adresser aux:

Editions de l'Ecole Polytechnique de Montréal
Ecole Polytechnique de Montréal
Case postale 6079, Succursale A
Montréal (Québec) H3C 3A7
(514) 340-4000

Compter 0,10$ par page (arrondir au dollar le plus près) et ajouter 3,00$ (Canada) pour la couverture, les frais de poste et la manutention. Régler en dollars canadiens par chèque ou mandat-poste au nom de l'Ecole Polytechnique de Montréal. Nous n'honorerons que les commandes accompagnées d'un paiement, sauf s,il y a eu entente préalable dans le cas d'établissements d'enseignement, de sociétés ou d'organismes canadiens.

LIST OF SYMBOLS

D	Pipe diameter
E	Average output voltage (Volt DC)
E'	Fluctuating component of output voltage (RMS)
m_s	Mass of empty container
m_{Li}	Initial mass of liquid alone contained in fully filled tube
m_{Lsi}	Initial mass of container fully filled with liquid
m_{Lf}	Final mass of liquid in tube after quickly closing the valves
T	Total sampling time
t_{Gi}	Width of conditioned wave of front sensor
U	Average flow velocity
u	Fluctuating component of average flow velocity
V	Volume
X_o	Flow volumetric quality (ratio of initial air flow rate to initial total flow rate)
v	Transversal direction
z	Axial of longitudinal direction
α	Local void fraction
$\delta(r,t,v)$	Phase indicative function corresponding to threshold level V

LIST OF TABLES

LIST OF FIGURES

CHAPTER I

INTRODUCTION

The presence of the dispersed phase in a continuous flow is characterised by the proportion occupied by this phase during the flow. In an air-water mixture flow, this proportion represents the quasi-static fraction of air bubbles and is symbolised by α. Since void fraction is a measure of the change in proportion resulting from a variation in the dispersed phase or from interaction between phases, it represents an additional independent kinetic variable in the general expression of a two-phase flow.

Void fraction is indispensable in the evaluation of average mixture density, average kinetic energy of phases, pressure drop, momentum and mass transfer rates as well as in the detailed study of the mechanism of a mixture flow. Important industrial applications such as nuclear and bubble column reactors in nuclear and chemical industries, for example, currently need more data on the local information of flow.

Most practical applications deal with turbulent flow in which a variety of flow regimes exist. Flow regimes make the flow more complicated and limit the versatility of instruments developed for measurement of different quantities of interest in two-phase flow.

Void fraction may be determined by several methods which have been proposed notably the use of a resistive probe (Neal and Benkoff [1]), a hot wire anemometer (Hsu et al. [2]) or hot film (Delhaye [3]), the gamma ray method (Kazin [4]), the optic tiper method (Miller and Metchie [5]) or lasers (Ohba et al. [6]) for the most part in air-water vertical flows.

In their results, Brown et al. [7] represent the void fraction profile of horizontal and vertical, bubble and slug, upward and downward flow in a tube the 2.5-in. diameter by equations of the parabolic type having a maximum value at the pipe wall. Zivi [8] expressed the rate of dissipation of energy of an annular flow in terms of the void fraction which is obtained after minimizing the dissipation of energy. Brown and Kranich [9] have obtained the void fraction and velocity profiles by simulating the modified conservation equations of a horizontal/vertical bubble flow in a 1.0-in. diameter pipe with measurements of pressure and overall liquid fraction. Measurements

in 3-D with a conical hot film probe have also been presented by Wang et al. [10] in small diameter vertical bubbly flow.

Parabolic form of void distribution in some previous work may be assumed for symmetrical flow such as, for example, flow in a radial plane and bubbly vertical flow.

A recent study by Yamazaki and Simizu [11] indicates the difficulty if not the impossibility of obtaining, in theory, the profile of the void fraction and then the phase velocities, based on two concepts: hydordynamic (3D-2V-1T) and hydraulic (1D-2V-2T) equations where D, V an T denote dimension, velocity and time, respectively. The nature and values of interaction forces within each phase in the former are generally unknowns. Elimination of these terms renders impossible the solution of the whole set of equations. The void fraction and pressure drop, however, could be obtained by a coherent hypothesis and non-theoretically. The number of variables in the latte exceeds the number of equations, the omission of interaction terms and consideration of the product of density and gravitational acceleration as constant reduce the flow to that of hypothetical case.

In this study, our main interest is the prediction of void fraction in a large diameter, horizontal, air-water mixture and highly turbulent pipe flow. To our knowledge little work has been done and no correlation of void distribution established in this kind of flow both in longitudinal and cross-sectional planes.

CHAPTER II

PRINCIPLE OF MEASUREMENT OF VOID FRACTION

2.1 Definition of void fraction

The principle of measurement of void fraction is illustrated in Figure 1. The passage of air bubbles through a sensor placed somewhere in a pipe is revealed by the different electric voltages compared with those gathered in the absence of bubbles. The use of an adjustable thereshold level of a discriminator circuit makes it possible to determine the local void fraction. Void fraction determined by this way is considered as the ratio of the average time of travel by the bubbles and the total measuring time, T, long enough for the time of travel of the bubbles to be equivalent to the width of conditioned rectangular of sinusoidal waves. These waves correspond to the passage of bubbles.

Void fraction can be defined in two ways:

* Local void fraction:

$$\alpha = \frac{\sum_{i=1}^{n} t_{G\,i}}{T} = \lim_{T \to \infty} \frac{1}{T} \int_{o}^{1} \delta(r,t,v_s)\,dt \qquad (1)$$

where $t_{G\,i}$: width of the conditioned wave (front sensor of a double probe).

T : duration of measurement of total sampling time

$\delta(r,t,V_s)$: phases indicative of functions corresponding to threshold voltage V.

$\delta = 0$ in absence of bubbles.

$\delta = 1$ in presence of bubbles.

* Global void fraction:

- Volumetric : $\bar{\alpha}_V = \Sigma V_i(t)/V$ or $\frac{1}{V}\int_V \alpha dv$

- Surface : $\bar{\alpha}_S = \Sigma S_i(t)/S$ or $\frac{1}{S}\int_S \alpha ds$ (2)

- Linear : $\bar{\alpha}_L = \Sigma L_i(t)/L$ or $\frac{1}{L}\int_L \alpha dL$

2.2 Use of hot film anemometer

Regarding local measurement of void fraction, each method of technique has certain advantages and disadvantages; for example, the laser anemometer is not used except for very weak concentrations of bubbles and in the conductivity method electric conductivity loses its meaning with strong concentrations of bubbles, etc.

A comparison of the optical probe, resistive probe and not film anemometer by Galaup [12] reveals that almost equivalent results Moujaes and Dougall [13] also found that local void

fractions measured using wedge type hot film anemometers were comparable to those obtained by optical fiber probes. Their experiment is performed in a large vertical rectangular channel of 12.7 x 76.2 mm cross-section.

The choice of measurement method is then a compromise between the different parameters of interest: price, availibility of measurement and analysis equipment, etc.

In this context, the hot film anemometer method is adopted here because of its current application in measurement of flow velocity, intensity of turbulence, void fraction and even temperature independent of different flow patterns.

Its of operating principle in two-phase flow is based on the difference in heat dissipation rates during the passage of phases through the probe (Hsu et al. [2], Goldschmidt and Eskinazis [14] and Delhaye [3]). The sensitivity of the hot film sensor depends, then, on the variations of velocity in an isothermic single phase flow and the change of phases in a two-phase flow, the heat transfer coefficient of the liquid phase being about two to three times that of the gas phase.

The arrival of a bubble on the sensitive element causes a slow reduction in the heat transfer rate which means less power is needed to maintain this element at constant temperature.

This power reduction is indicated by a decrease in output voltage of the hot film anemometer. The situation becoming the normal as the bubble disappears and the output tension rises rapidly. The hot film probe is shown to be a good measurement instrument because of its rapid response to the passge of a bubble.

Fluctuating signals turnished by the hot film anemometer are then passed through a series of amplifiers, filters and the electrical circuit of a discriminator. Their outputs are conditioned signals which make if possible to determine the average value of the local void fraction. This value needs, however, to be compared with that obtained by a global measuring method such as quick closing valves.

CHAPTER III

EXPERIMENTAL SETUP

3.1 Vertical calibration loop

This loop is designed to perform the calibration of the hot film probe for measuring the void fraction, as shown in Figures 2.a and 2.b.

It consists of a series of steel and plexiglass pipes where a continuous current of water is delivered to the base of the vertical part of the loop water is supplied by a 50 HP centrifugal pump with an initial water flow rate of maximum 1600 USGPM. Compressed air at 50 psig is injected in to a cylindrical mixing chamber 2.0-in. in diameter and 4.0-in. in length, where a two-phase air-water flow is produced through a series of 80 1/8-in. holes pierced along the perimeter.

Water and air flow rates are controlled by a monitoring valve and a series of air filters & pressure regulators at constant pressure (5 psig to 125 psig/respectively).

The calibrated section consists of a clear vertical pine 2.0 inches in internal diameter and 40 inches in length which can be closed instantaneously by means of two quick-closing valves with the same section as that of the pipe. The valves present no

restriction in the open position and the connecting parts are carefully made so as to avoid any kind of flow perturbation.

An air pressure regulator of 90 psig maximum, called the speed control box, controls the open/close velocity of the two valves that are activated by means of a rigid mechanical connection.

In normal operating conditions, the inlet air pressure of the box is regulated at about 65 psig which corresponds to a sufficiently, short response time, less than 0.5 sec. to avoid any irregularities which could result while the two valves are being manoeuvered.

Visual observations at the test section indicate that the flow is already stable at 42 times the pipe diameter from the mixing chamber. Also, preliminary analysis of signals recorded across the pipe reveals in a quantitative way the symmetry and homogeneity of flow, and the verticality of the test tube.

Air and water temperatures are controlled by means of regular thermometers. After passing through the flow circuit, the mixture is collected in a separating tank, where the water is sent back to the pump while air bubbles escape freely in to the surrounding atmosphere.

3.2 Horizontal test loop

Experiments were performed in a horizontal closed loop which has been described by Lakis [15]. A large horizontal flow circuit is fed by a centrifugal pump of 150 HP two centritugal pumps of 75 HP each. This pumping system feeds the loop at a rate of 2000 to 5000 USGPM from a 15000 USG reservoir tank water flow rates are regulated as they pass through a closed 2500 USG pressure vessel, and then through a mixer of 2000 holes 3.0 mm in diameter where compressed air is injected to produce a two-phase flow.

This mixture finally runs through a horizontal pipe 1360 feet in length and returns to the open reservoir. The experimental section consists of a series of PVC, steel and plexiglass pipes of 8.0-in. nominal diameter, schedule 80.

Water and air flow rates are controlled by precalibrated orifice flow meters which are connected respectively to their differential Hg and H20 manometers.

Temperatures of air and water are indicated by well-protected thermometers placed at the entrance to the mixer and near the loop exists.

Several pressure taps placed along the pipe permit in measurement the pressure drop. In addition, 3 equidistant holes 10/32 in. In diameter were made around one-half of the pipe perimeter, from the top to the bottom. Picked up piezometric lines are essential for controlling the stability and reproductibility of the measurement conditions in both single and two-phase flows.

Finally, a central line was drawn at each axial measurement location (top side of the pipe) to racilitate the alignment of the probe. This alignment ensures that the axial direction of the sensor placed in the pipe is parallel to that of the pipe and hence the flow. The up and down motion of the sensor's support is controlled by means of a tranverse mechanism.

3.3 Experimental conditions

Flow patterns depend fundamentally on the initial flow rates or the superficial velocity of each constituent phase.

Several investigators have proposed a variety of flow maps corresponding to specific flow. There are graphic representations in different forms where flow patterns may be identified by superficial velocities (Govier and Omer [16], Taitel and Duckler [17], Mandhane et al. [18], Sekoguchi et al. [19], Barnes et al. [20]), by ratio of volumetric flow rate to Froude

number (Golan and Stenning [21]), or by enregy spectrum of phases (Hubbard and Duckler [22], Hewitt and Roberts [23], Chisholm [24], etc.

According to Savery [25], flow patterns in air-water horizontal flow with liquid predominating are very different and depend on the given initial flow rate of the continuous phase. Also, measurements performed in two diferent horizontal pipes, 2.54 and 9.53 cm in diameter ([26]) indicate the complexity of the transition mechanism for the same flow conditions.

In this study, visual observations of flow patterns agree more or less with those of Mandhane et al. [18] and Hoogendoorn [27] whcih are the easiest to compare. However, the choice of flow volumetric quality, X_o (ratio of gas volumetric flow rate to total volumetric flow rate) for current experimental work is limited by the loop capacity. Practical applications demand more accurate flow identification.

For this purpose, selected experimental conditions are given in Table 1, a flow map generated in fully developed flow conditions and observed flow patterns are illustrated in Figures 4 and 5 / respectively.

CHAPTER IV

APPARATUS AND EXPERIMENTAL PROCEDURE

4.1 Hot film probe and its support

A double conical hot film probe was designed to simultaneously measure a pair of passing bubble signals. The first siganl, given by the front sensor, provides void fraction information. Both front and rear signals are used to determine the local linear velocity of the bubbles.

The choice of a conical form has the advantage of preventing the deposity all impurities, particles or filaments in suspension in the water which may deform of even break the sensor and also prevents fatigue failure due to excessive vibration produced by vortex shielding which may occur with a cylindrical form.

The probe consists of two very thin films of platinum and a thin dielectric layer. The films thickness is nearly 0.1-in. In providing the fissuration of platinum films and their quartz coating, the films have been designed with stable characteristics in time, i.e. without resistance variation in even cold temperatured as well as being able to prevent contamination or erosion without significant change to the response.

The separate distance 'd' between two films is estimated in determining the mean diameter of air bubbles 'd_G' at the clear test section by cinematography optimum values of 'd' and 'd_G are 3.03 mm and 2 to 3 mm. respectively.

The probe was made by TSI Company and is shown in Figure 6. Its rigid support as shown in Figure 7 may be positioned accurately in the flow. It is made up of:

- A helicoidal endless screw displacement mechanism.
- A vertical adjustable scale for compensating the number of threads in the pipe orifice once the probe is screwed in.
- Two big screws of the clamp type for attenuating the vibration of the probe support, especially when the probe is in the lower part of the pipe of at high flow rates.
- A directional indicator to ensure that the direction of the sensor placed in the pipe and that of the flow are the same.

4.2 Calibration procedure

The calibration procedure includes calibration of the hot film sensor in both single phase water flow and two-phase flow, calibration of the magnetic recorder and the electric circuit of the discriminator, and verification of related accessories.

4.2.1 Calibration of magnetic recorder

Linearity of the continuous component of recorded signals and minimum distorsion of response are necessary for obtaining results with good amplitude precision. This requires that the signal be recorded in relatively high signal to noise ratio conditions.

A source of white noise connected to a frequency analyzer (Special Dynamic analyzer II, SD 375) is used as the input signal of a magnetic recorder. Recording of input signals is carried out simultaneously on 4 channels of the recorder under the following conditions:

Magnetic tape : high precision Ampex tape, 3 simultaneous data recording channels (max. 35 mm. thickness and 6.25 mm. width).

Recorder : Racal Store 4 DS, portable, 3 FM channels and 1 DR channel, FM wideband (record mode).

Tape speed (in/sec.)	Bandwidth (kHz)		Signal to noise (dB)	Carrier deviation (%)
3 3/4	0	2.5		
7 1/2	0	5.0	48	+ 40
15	0	10.0		

The output frequency spectrum ensures the fidelity of recorder up to 20 kHz as shown in Figure 8.

4.2.2 Calibration of hot film in water flow

A hot film anemometer can be operated in two ways:

1. At constant intensity: measure film resistance at a constant current.
2. At constant temperature: measure necessary current to maintain constant temperature of film, hence its resistance.

The former is rarely used owing to complications introduced by the necessity for compensating the resulting variations of heat exchange between the sensitive element and its support (Resch and Coantic [20], Bouvard and Dumas [29]).

In order to limit the temperature of the sensitive element to the lowest possible value with respect to sensitivity preemptions, the overheat coefficient corresponding to the film in water at 80°C calculated and found to be equal to about 1.1.

Calibration of the hot film in water is schematically shown in Figure 9. Conditions in which two different models of hot film were calibrated are also given in Table 2.

The calibration procedure may be summarized as follow:

- Disconnect the probe from the cable ($\simeq$ 5 m) and put the extrtemity of the cable in short-circuit, balance the bridge with a potentiometer until it measures R = 0.
- Dip the cold probe in static water (actually with a continuous current of very low flow rate in order to avoid the formation of bubbles on the heated element, and to maintain the water temperature at T° amb $\pm$ 0.05° C). Rebalance the bridge with the probe resistance. Decrease the resistance of the probe and its accensory from the value which was to be balanced previously.
- Correct this value with the calculated overheat ratio. The final value represents the functioning resistance of the hot film.
- Start the servo amplifier and obtain output voltage by means of a voltmeter.

In spite of an advantageous geometry, Morrow [30] demonstrated experimentally that the accumulation of impurities at the film surface might reduce the heat transfer rate; the output voltage possibly may not therefore being uniquely a function of velocity or the temperature of the fluid. for this reason, the

probe is carefully cleaned with alcohol and distilled water before and after use.

According to Davies and Patrick [31], for a high Reynolds number ($>10^5$), the output voltage of the anemometer, the sensitivity of the film and the intensity of turbulence may be expressed as:

- Output voltage : $$E^2 = A + BO^{1/2} + CU \quad (3)$$

- Sensitivity of film : $$\frac{dE}{dU} = \frac{BU^{-1/2} + 2C}{4E} \quad (4)$$

- Intensity of turbulence :

$$\frac{\sqrt{\overline{u^2}}}{U} = \frac{8CE\sqrt{E'^2}}{B^2 + 4C(E^2 - A) - B(B^2 - 4C(E^2 - A))^{1/2}} \quad (5)$$

Where
- E : average tension (volt DC)
- E' : fluctuating component of E (RMS)
- U : average flow velocity
- u : fluctuating component of U
- A,B,C : unknown constants

With the results of (3), (4) and (5), the calibration curve of the front film of probe, model 1231 AF W, was platted and is given as an example in Figure 10. The dynamic sensitivity of hot film and intensity of longitudinal turbulence are also given in Table 3.

4.2.3 Calibration of hot film in two-phase flow

This step is carried out in the vertical calibration loop for this simple reason: determination of void fraction by quick closing valves in real 8-in. diameter test pipe is impracticable because the existing valves are undersized and more particularly because of the pressure effects exercised by the flow.

Calibration of hot film in two-phase flow is schematically shown in Figure 11. Details on calibration procedure are also illustrated in Figure 12.

In Figure 12, signals delivered by the front film of a conical double probe pass through a discriminator circuit, the output of which is a rectangular wave of equivalent height to that of an adjustable threshold. The maximum threshold height corresponds to 1 V for the output signal preadjusted to 2 V peak to peak from the recorder. A time meter connected to the output of the circuit provides the sum of rectangular widths in sec. or milisec. onds. The ratio of this sum to total sampling time is equivalent to the average local void fraction. The numbr of rectangular waves measured by a frequency meter during a given sampling time represents the bubble impact rate.

Apparatus and experimental conditions are almost the same in both calibration and test phases. Amplification and attenuation

of recorded signals was achieved with Ithaco 451 amplifiers or the Hewlett Packard 350D attenuator.

4.2.3.a Discriminator circuit

The discriminator circuit snown in Figure 13 was constructed and tested with rectangular or sinusoidal waves at various known frequencies. For calibration and measurement, the total time of a given sample was counted by a chronometer. The average absolute errors in the determination of wave width and number or waves in the range of < 2.5 kHz were 0.3 % and 0.1 %, respectively, where:

$$\text{Absolute Error} = \frac{1}{n} \Sigma \left| \frac{\alpha_{known} - \alpha_{mes.}}{\alpha_{known}} \right| * 100$$

4.2.3.b Choice of optimum threshold

Referring to Figure 12, when each signal v (t) obtained at given radial position passes through the discriminator, for each value V_D of interest that one can choose from an adjustable voltage level of the threshold, the corresponding output at the time meter during a sampling time T is the sum $(\sum_{i=1}^{m} t_{Gi})_{Dj}$. Repeating the same procedure with various values of voltage level V_D, a graph indicating the variation of with V can finally be drawn. The function in the graph may be divide approximately in to two parts, and named part A and part B. Part A is established when the threshold is found in the zone dominated by the

gas phase. The zero value of $\Sigma t_{G\,i}$ indicates there is no bubble signal detected by the threshold and is normally the starting point of the function. Part B is established when the threshold moves up slowly near the liquid voltage level and represents the peaks resulting not only from the passage of bubbles but also from the fluctuation of the liquid phase itself and supplementary fluctuation due to bubble agitation.

The degree of perturbation varies within flow patterns and from one radial position to another. The critical point between parts A and B is judged byvisually examining the signals with a special oscilloscope. The judgement is based on whether or not there is a significant change in $\Sigma t_{G\,i}$ (as indicated by the time counter) between two successive values of V_D, for the same small increment.

Now, in repeating the same procedure for various radial positions, various values of α_{ind} will be obtained where:

$$\alpha_{ind} = \frac{\left[\sum_{i=1}^{m} t_{G\,i}\right]_{D\,j}}{T} \qquad (6)$$

α_{ind} represents the local void fraction determined by the not film technique (indirect method). Correction will be made by comparison with the void fraction obtained by the global or direct method.

By performing the numerical integration of all α_{ind} evaluated for one value of flow volumtric quality, X_o, on the volume of the pipe (tube of calibration loop), I_1 can be obtained. Also, the direct method that will be discussed her one value α_{dir} for the same value of X_o.

If the flow is homogeneous and the distribution of α_{ind} is uniform at all points in the volume, the equality $I_1 = \alpha_{ind}$ indicates that the choice of threshold level is correct.

Evaluation of signals indicates the bubbles are spread in a symmetrical way and almost uniform in the calibration section.

4.2.3.c Global method

This method consists of measuring instantaneously the volume of water in an air-water flow mixture and deducing the volume of air, the result representing the volumetric void fraction.

The volumes of water contained in the tube before and after quickly closing the valves may be defined as:

- Initial : $V_{Li} = \frac{m_{Lsi} - m_s}{\rho_L}$

- Final : $V_{Lf} = \frac{m_{Lsf} - m_s}{\rho_L}$

where : m_s : mass of empty container (606.9 gr)

m_{Lsi} : mass of container and initial liquid (valves in open position) (3075 gr.)

m_{Lsf} : mass of container and final liquid (after closing two valves)

ρ_L : density of water.

If α_v is the ratio of final air volume found in the tube to total volume of water in the fully rilled with tube, we must have:

$$1 - \alpha_v = \frac{V_{Lf}}{V_{Li}}$$

with

$$\alpha_v = \frac{m_{Lsi} - m_{Lsf}}{m_{Lsi} - m_s} \qquad (7)$$

or

$$\alpha_v = 4.052 * 10^{-4}(3075 - m_{Lsf}) \qquad (8)$$

In practice, the volumetric void fraction, α_{dir}, is obtained by taking the average value of some α_v. The reproducibility of results depends on the response of the closing mechanism; two to three values of are reasonable in general. The time necessary for the flow to be stable after each closure is about 15 minutes.

Electronic equipment used to determine the void fraction is snown in Figure 14. The calibration curve for the void fraction is given in Figure 15, where a linear relationship was found to exist between measured void fractions by quick closing valves and those by not film.

Figure 16 illustrates an example of a void fraction determined by the hot film & discriminator technique over a period of 160 sec. Some other examples of the determination of void fractions in a large pipe (horizontal test loop) are also given in Figure 17, where tests were carried out at various flow volumetric qualities. X_o, and with axial location, z/D.

In a large pipe, the choice of threshold level is delicate for measurements hear the upper pipe wall because very a strong fluctuation (vortex of flow may exist in the space of the pipe orifice when the probe is not completely placed along the height of this orifice) and several samples and arduous examination of signals are required; measuring time is normally 4 to 5 times longer than that at positions far from the upper wall in order to facilitate judgement on an average value.

The difference in reproducibility of measurements taken under the same experimental conditions but at different moments is 10 to 15 % for positions nesar the upper wall and about 10 % for others.

CHAPTER V

RESULTS AND PROPOSED CORRELATIONS

Experiments are first of all carried out at the pipe centre line and along 24 equidistant axial locations on a total length of 170 times pipe diameter from the mixer. Local void fraction distributions are obtained in measuring through both transversal and radial planes at each axial location, where 9 radial positions are defined for each cross-sectional plane. The average time giving statistically significant local measurement is 3 to 5 minutes. In order to verity the reproducibility of results, all local measurements are performed at least 3 times under the same experimental conditions.

5.1 Longitudinal distribution of void fraction

The variation of measured void fraction at the centre line of the pipe with axial locations, performed for a differnet flow volumetric quality, X_o, is given in Figure 18.a. No major change in value was noted except from axial location $z/D \geq 100$ where the flow is supposed to be fully developed near the mixer, $z/D = 38$, the void fraction profile (not shown here) mixing performance of the mixer, but the unifromity changes gradually douwnstream. Examples of void fraction profiles taken at clear sections downstream and at nighest water flow rate can be seen

in figure 18.b. In this figure, the uniformity of profile changes when X > 0.116; from axial location z/D = 92, the profile changes completely with as increase in X_o. Visual observations of flow also indicate there is a strong accumulation of bubbles in the upper half of the pipe and a relatively small one in the lower part (Figure 5).

It may be said, that the flow perturbations manifested from the exits of the mixer to test a downstream section at a sufficiently high air flow rate. They greatly influence the void fraction profile which in turn influences the profile of other flow parameters.

The longitudinal distribution of void fraction also indicates that void fraction is a function both of volumetric quality, X_o, and axial location, z/D.

In normalizing the measured void fraction at the pipe centre line at different axial locations, α , with respect to those at the pipe centre line of fully developed flow, α_{FD} , (z/D > 130), the longitudinal distribution of void fraction may be assumed to be:

$$\frac{\alpha_{\ell}}{\alpha_{FD}} = A\ (z/D) + B \qquad (9)$$

where α_{ℓ} : measured void fraction at pipe centre line of each axial location z/D

$\alpha_{FD\ell}$: measured void fraction at pipe centre line of fully developed flow, z/D > 130

z : pipe length measured from mixer

D : nominal diameter of pipe

A,B : unknown constants.

Furthermore, constants A and B may be expressed in terms of flow volumetric quality, X_o, as follows

$$A = A_1 X_o + A_2$$

$$B = B_1 X_o + B_2$$

where $$X_o = \frac{\text{initial air volumetric flow rate}}{\text{initial "air+liquid" volumetric flow rate}}$$

A_1, A_2, B_1, B_2 : unknown constants.

Constants A_1, A_2, B_1 and B_2 are finally determined by linear regression wher (9) can be written as:

$$\frac{\alpha_\ell}{\alpha_{FD\ell}} = (0.015\ X_o - 0.009)(z/D) + (-1.88\ X_o + 2.03) \quad (10)$$

Comparison of calculated values from (10) with experimental results given in Figure 19.

5.2 Cross-sectional distribution of void fraction

In order to obtain a true image of void fraction profile in a large diameter horizontal pipe, measurements were performed through 9 radial positions in each cross-sectional plane. At the highest flow rate (water normally), measurements in the

lower part of the pipe were sometimes achieved separately after experiments in the ubber part were terminated. the probe placed in the pipe flow may be considered as a clamped, free beam in a vibration field. Vibration of the probe itself could interfere with the data collection and easily damaged the sensor. The rigidity of probe traversing mechanism and that of the sensor support, the existence of particles in suspension, the direction of the sensor in the flow and any source of vibration are demand a great deal of attentions during experimentation.

5.2.1 Transversal plane

Void fraction profiles in the transversal plane measured at axial location z/D = 130 are given in Figure 20.a. functional dependence of void profile expressed in terms of flow volumetric quality, X_o, and axial location, z/D, is shown in figures 21.a and 21.b, respectively.

Variation of local void fraction with flow volumetric quality X_o, is also examined at different radial positions; the results for three axial locations downstream are given in Figure 21.c.

Through them, the non-uniformity of the profiles (i.e. caused by phase separation) indicates the curves represent

heither a parabolic nor a power distribution law as usually proposed symmetrical or vertical flows.

As it is not always easy to obtain reliable measurements in the vicinity of the pipe wall, values at the wall would be supposed in such way that correlations may be easily and reasonably established. In other words, the prediction models will be valid for measurements carried out in the range of $0.555 < y/D < 0.945$, where y/D is normalized distance measured from the upper part of the pipe.

Furthermore, most of the water is in the lower part of the pipe where air bubbles are practically non-existent, as previously indicated by visual observation of flow even at nearly 30% maximum flow volumetric quality.

Void fraction can then be considered as having a zero value at the lower wall ($y/D = 1$). In the upper part of the pipe ($y/D = 0$) where air bubbles are normally concentrated, void fraction is assumed, for instance, to be zero although it probably has certain non-zero values.

After several attempts, it was found that the distribution of void fraction in the transversal plane may be predicted by the two proposing following models:

* Model 1 : The void profile is approximated by linear functions such as:

$$\alpha = A_1 \, (y/D) + B_1 \quad (0.0 \leq y/D \leq 0.6)$$

$$\text{and } \alpha = A_2 \, (y/D) + B_2 \quad (0.6 \leq y/D \leq 1.0) \qquad (11)$$

The constants A_1, A_2, B_1 and B_2 are determined by linear regression where finally (Figure 22):

$$\alpha = -3.33 \, (y/D) + 2.37 \quad (0 \leq y/D \leq .6)$$

$$\alpha = -1.36 \, (y/D) + 1.59 \quad (.6 \leq y/D \leq 1) \qquad (12)$$

This model gives the non-zero values at the pipe wall.

* Model 2 : Using the assumption of zero values of void fraction at the pipe walls, void profile is assumed to have the form of the product of power and exponential functions, such as:

$$\alpha = (y^{*a} - y^{*}) e^{-by^{*}} \qquad (13)$$

where $y^{*} = y/D$ (same definition as above)
a and b are unknown constants.

Constants a and b determined by regression are:

$$b = 1 \quad \text{and} \quad a = e^{-8.046 X_o} \quad \text{(figure 23)}$$

(13) can be rewritten finally as:

$$\alpha = y^{*} \, e^{-y^{*}} \, (y^{* \, e^{-8.46 X_o}} - 1) \qquad (14)$$

Comparison of predicted values by two models and experimental results is shown in Figure 24, where:

	Arithmetic mean deviation	Standard deviation
* Model 1 :	1.7 %	3.5 %
* Model 2 :	4 %	3.3 %

5.2.2 Radial plane

Measurements of void fraction in the radial plane are carried out in the same way as those in transversal plane. An example of void profiles measured in fully developed flow (z/D = 110 and 130) at various flow volumetric quality, X_o is given in Figure 20.b.

Gravity theoretically has no effect on the variation of flow parameters or phase separation in this plane, therefore the profiles are symmetrical and behave like those of most of vertical flows.

The void fractions are distributed almost uniformly through the cross-section of the pipe.

However, the profile appears to become concave as flow volumetric quality, X_o, increases. This implies that the given flow would probably be annularly dispersed in a moment with a strong concentration of air bubbles along the pipe perimeter.

Values of void fraction in this plane are found to be nearly equal to those near pipe axis.

Because the form of the profiles is similar to that of velocity distribution in turbulent water flow, the power law may be assumed for the distribution of void fraction in a radial plane where:

$$\frac{\alpha}{\alpha_{\ell}} = a \cdot (1 - |2y^* - 1|)^b \qquad (15)$$

where α_{ℓ} : measured void at pipe axis

$y^* = y/D$: normalized distance measured from wall

a and b are unknown constants.

Similarly, regression analysis gives finally:

$$\frac{\alpha}{\alpha_{\ell}} = 1.0 \ (1 - |2y^* - 1|)^{0.011} \qquad (16)$$

Comparison of predicted values obtained by (16) and experimental results is shown in Figure 25 (arithmetic mean deviation = 0.5 %, standard deviation = 1.5 %).

In both transversal and radial planes, the void fraction profiles are qualitatively comparable with those obtained numerically by Brown and Kranich (9) in linear pipe with Re = 175,000.

CHAPTER VI

CONCLUSION

Distribution of void fraction was investigated in the axial direction and in cross-sectional planes of a pipe with the help of the hot film anemometer. The use of hot film with a discriminator circuit has been shown to be a good technique for determining the local void fraction in small diameter pipes. However, its indicative values need to be compared with those obtained by a global method in order to approach the definition of void fraction.

A vertical calibration loop was constructed to calibrate the hot film in a symmetrical bubbly flow. The calibration curve indicates a linear relationship between void fractions determined by the hot film method and those obtained by the quick-closing valves method. This curve, which is valid only for the one hot film under consideration is used to correct the values measured by the hot film in large diameter pipes.

Experimentation in a horizontal test loop indicates that difficulty sometimes arises in the choice of an optimum threshold level, especially in dealing with signals recorded in the near wall region (< 1 in. from wall). An average value of the

threshold was taken after 6 measurements which was considered reasonable, in this study. Outside this region, the fluctuation of the signal due to the passage of air bubbles is more obvious and the threshold can be more easily determined.

New correlations were proposed to predict the distribution of void fraction along, and in both, cross-sectional planes of the pipe. In the longitudinal direction, void fraction can be linearly expressed in terms of axial location and flow volumetric quality. In the radial plane, void fraction profiles are symmetric and similar to those of vertical flow, the power law being perfectly applied in this case. In the transversal plane, the profiles are asymmetric and in turn affect the phase distribution and mixture velocities. Void fraction distribution in this plane may be predicted either by the linear model or by the power & exponential model. It was also found that the profiles are qualitatively similar to those obtained in small diameter pipe horizontal flow. The effect on phase separation by gravity is dominant compared to that of turbulent bubble diffusion in the tranversal plane.

REFERENCES

[1] NEAL, L.G., BANKOFF, S.G., "A High Resolution Resistive Probe in Gas-Liquid Flow", AICHE, J., Vol. 9, 490-494, 1963.

[2] HSU, Y.Y., SUMON, F.F., GRAHAM, R.Q., "Application of Hot Wire Anemometry for Two-Phase Flow Measurements such as Void Fraction and Slip Velocity", Prepared for ASME Winter Meeting, Philadelphia, 17-22, Nov. 1963.

[3] DELHAYE, J.M., "Anémomètre à flm cc ud dans les écoulements diphasiques. Mesure du taux de présence du gaz", C. R. Acad. Sc. Paris, t.266, série A, 370-373, février 1968.

[4] KAZIN, I.V., "Radial Distribution of Vapor in Upward Turbulent Steam Water Flow", Teploenergetika, Vol. 1, 40-43, 1964.

[5] MILLER, N., METCHIE, R.E., "The Development of a Universal Probe for Measurement of Local Voidage in Liquide/Gaz Two-Phase Instrumentation", Proc. 11th Nat. ASME/AICHE Heat Transfer Conf. on Two-Phase Instr., Minneapolis, Minnesota, 82-88, 1969.

[6] OHBA, K., KISHIMOTO, I., OGASAWARA, M., "Simultaneous Measurement of Local Liquid Velocity and Void Fraction in Bubbly Flows Using a Gas Laser - Part II. Local Properties of Turbulent Bubbly Flow", Technol. Rep. Osaka Univ., Vol. 27, No. 1358, 228-238, Mars 1977.

[7] BROWN, R.W., GOMEZPLATA, A., PRICE, J.D., "A Model to Predict Void Fraction in Two-Phase Flow", Chemical Engineering Science, Vol. 24, 1483-1489, 1969.

[8] ZIVI, S.M., "Estimation of Steady State Steam Void Fraction by Means of the Principle of Minimum Entropy Production", J. of Heat Transfer, Trans. ASME, Serie C, Vol. 86, 247-252, May 1964.

[9] BROWN, F.C., KRANICH, W.L., "A Model for the Prediction of Velocity and Void Fraction Profiles in Two-Phase Flow", AICHE J., Vol. 14, 750-758, September 1968.

[10] WANG, S.K., LEE, S.J., JONES Jr, O.C., and LAHEY Jr, R.T., "3-D Turbulence Structure and Phase Distribution Measurements in Bubbly Two-Phase Flows", Int. J. Multi-phase Flow, Vol. 13, No. 3, 327-343, 1987.

[11] YAMAZAKI, Y., SIMIZU, M., "Hydrodynamic and Hydraulic Studies on Void Fractions in Two-Phase Flow", J. of Nuclear Science and Technology, Vol. 15, No. 12, 886-898, December 1978.

[12] GALAUP, J.P., "Contribution à l'étude des méthodes de mesure en écoulement diphasique", Thèse de Doctorat, Université de Grenoble, 1975.

[13] MOUJAES, S., DOUGALL, R.S., "Experimental Investigation of Concurrent Two-Phase Flow in a Vertical Rectangular Channel", The Canadian J. of Chem. Eng., Vol. 65, 705, October 1987.

[14] GOLDSMHMIDT, V., ESKINAZI, S., "Two-Phase Turbulent Flow in a Plan Jet", J. of Applied Mechanics, Vol. 33, No. 4, 735-747, 1966.

[15] LAKIS, A.A., "Numerical Analysis of Wall Pressure Fluctuations in Two-Phase Flow", Proc. of 5th International Conference, 17th - 21st, University College Swansea, U.K., 757-767, 1978.

[16] GOVIER, G.W., OMER, M.M., "The Horizontal Pipeline Flow of Air-Water Mixtures", The Canadian J. of Chemical Eng., 93-104, June 1962.

[17] TAITEL, Y., DUKLER, A.E., "A Model for Predicting Flow Regime Transitions in Horizontal and Near-Horizontal Gas-Liquid Flow", AICHE J., Vol. 22, 47-55, 1976.

[18] MANDHANE, J.M., GREGORY, G.A., AZIK, K.A., "A Flow Pattern Map for Gas-Liquid Flow in Horizontal Pipes", Int. J. Multiphase Flow, Vol. 1, 537-553, 1974.

[19] SEKOGUCHI, T., AKAGAWA, K., HAMAGUCHI, H., IMOTO, M., ISHIDA, S., "Flow Regime Maps for Developing Steady Air-Water Two-Phase Flow in Horizontal Tubes", Mem. Fac. Eng. Kobe Univ., Vol. 25, 191-202, 1979.

[20] BARNEA, D., SHOHAN, O., TAITEL, Y., DUCKLER, A.E., "Flow Pattern Transition for Horizontal and Inclined Pipes: Experimental and Comparison with Theory", Int. J. of Multiphase Flow, Vol. 6, 217-225, 1980.

[21] GOLAN, L.P., STENNING, A.H., "Two-Phase Vertical Flow Maps", Proc. Instn. Mech. Engrs., Vol. 184, Part 3C, 108-114, 1969-1970.

[22] HUBBARD, M.G., DUCKLER, A.E., "The Characteristization of Flow Regimes for Horizontal Two-Phase Flow", Proc. of the 1966 Heat Transf. and Fluid Mech. Inst., Stanford, 100-121, 1966.

[23] HEWITT, G.F., ROBERTS, D.N., "Studies of Two-Phase Flow Patterns by Simultaneous X-Ray and Flash Photography", A.E.R.E., M. 2159, 1969.

[24] CHISHOLM, D., "Flow Pattern Maps in Horizontal Two-Phase Flow", Int. Conf. on the Physical Modelling of Multi-phase Flow, Coventry, Great Britain; Communication F1, 219-232, 19-21 April 1983.

[25] SAVERY, C.W., "Flow Patterns in Two-Phase Flow", The Symp. on Polyphase Flow and Transport Technology, Century 2 Emerging Technology Conf., San Francisco, CA., ASME, 75-88, 13-15 August 1980.

[26] LIN, P.Y. HANRATTY, T.J., "Effect of Pipe Diameter on Flow Patterns for Air-Water Flow in Horizontal Pipes", Int. J. Multiphase Flow, Vol. 13, No. 4, 549-563, 1987.

[27] HOOGENDOORN, C.J., "Gas-liquid Flow in Horizontal Pipes", Canadian J. of Chemical Eng. Sci., Vol. 9, 205-217, 1959.

[28] RESCH, F., COANTIC, M., "Etude sur le fil chaud et le film chaud dans l'eau", La Houille Blanche, No. 2, 151-161, 1969.

[29] BOUVARD, M., DUMAS, J., "Application de la méthode de fil chaud à la mesure de la turbulence dans l'eau", La Houille Blanche, No. 3, 257-270, No. 7, 723-734, 1967.

[30] MORROW, T.B., "Effects of Dirt Accumulation on Hot Wire and Hot Film Sensors", Fluid Dynamic Measurement : Discussion - Conference Papers, Vol. 1, 122-124, 1972.

[31] DAVIES, T.W., PATRICK, M.A., "A Simplified Method of Improving the Accuracy of Hot Wire Anemometry", Third Dynamic Measurement Conference Papers, Vol. 1, 152-155, 1972.

AIR

T_G= 24°C ± 2°C, P_G = 50 psig, ρ_G = 0.255 lbm/ft^3

WATER

T_L= 19°C ± 2°C, P_L = 1 atm, ρ_L = 62.4 lbm/ft^3
ν_L = 1.088 * 10^{-5} ft^2/ sec.

Q (ft^3/min)	U (ft/sec)	X_o	Q_{Lo}(USGPM)	U (ft/sec)
76.6	4.03	.116	4373	30.74
73.8	3.88	.131	3666	25.77
147.6	7.76	.219	3940	27.69
209.8	11.03	.264	4373	30.74
202.2	10.63	.292	3666	25.77

$$X_o=\frac{Q_{Go}}{Q_{Go}+Q_{Lo}},\ Q_{Go}=19.02*U_{Go},\ Q_{Lo}=142.26*U_{Lo},\ \rho_G=\frac{2.698*(PSIG)}{459.69+^\circ F}$$

ID = 7.625 in, Re_L(max) = 2 * 10^6, Mach(max)= 0.014 (<0.2, incompressible)

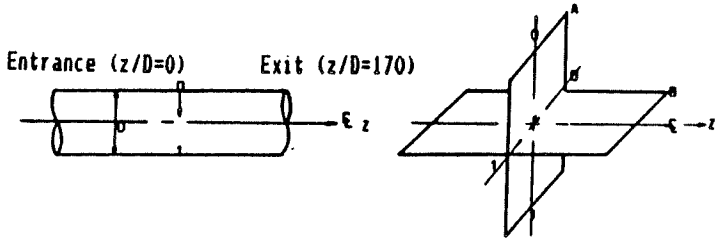

* 24 axial locations.
* 9 radial positions (tranversal plane A and radial plane B).

Table 1 Experimental conditions

Probes	position	T_{AMB}(°C)	T_{WATER}(°C)	R_{WATER}(Ω)	R_o(Ω)	T_{SC}(°C)	r(Ω)	C_S(/°C)	R_{SC}(Ω)
1231	Front	22.0	18.5	4.78	5.05	66.7	0.12	$2.2542*10^{-3}$	5.17
AK-W	Rear	22.0	18.5	4.37	4.58	66.7	0.12	$2.1372*10^{-3}$	4.69
1231	Front	20.0	17.5	7.60	8.16	66.7	0.15	$2.5778*10^{-3}$	8.39
AM-W	Rear	20.0	17.5	3.78	3.97	66.7	0.15	$2.5078*10^{-3}$	4.08

Ro : Normal operating resistance (Ω)
T_{SC} : Overheat temperature of hot film (°C)
r : Total resistance of probe except sensitive element
C_S : Sensitive coefficient of hot film

$$C_S = \frac{R_{100°} - R_{0°}}{100(R_{0°} - R_{int})}$$

où $R_{100°}$: Resistance at 100° C (Ω)

$R_{0°}$: Resistance at 0° C (Ω)

R_{int} : Internal resistance of hot film (Ω)

R_{SC} : Functioning resistance, charge $R_{SC} = (R_{EAU} - r)(1 + C_S(T_{SC} - T_{WATER}))$

avec $1 + C_S(T_{SC} - T_{WATER})$ = Overheat ratio

Table 2 Calibrating conditions of hot film in water flow (0 ≃ 0 ft/sec)

E(V)	$U_{L_{1-p}}^{-1/2}$ $\left(\sqrt[4]{\text{ft/sec}}\right)$	$(dE/dU_{L_{1-p}})$	$D=B^2+4C(E^2-A)$	$\sqrt{D}$	$\sqrt{e^2}$ (mV)	$\frac{\sqrt{u^2}}{U_{L_{1-p}}}$ $\left(\frac{mV}{ft/sec}\right)$
1)1.600	0.5	0.10115	1.9224	1.3865	1.6	4.6037
2)2.120	0.315	0.03797	1.0250	1.0124	2.7	7.0309
3)2.365	0.224	0.01712	0.5151	0.7177	4.5	13.2191
4)2.373	0.220	0.01632	0.4974	0.7053	4.6	13.6335
5)2.376	0.218	0.01593	0.4908	0.7006	4.7	13.9789
6)2.445	0.188	0.01009	0.3365	0.5801	5.9	19.5794
7)2.460	0.180	0.00859	0.3024	0.5499	6.5	22.3236
8)2.473	0.172	0.00713	0.2726	0.5221	6.9	24.5271
9)2.475	0.171	0.00694	0.2680	0.5177	7.0	25.0243
10)2.480	0.170	0.00675	0.2565	0.5065	7.1	25.7618

Table 3 Sensitivity of hot film and intensity of turbulence (A = 0.04, B = 1.76, C = 0.12, procedure of [30]).

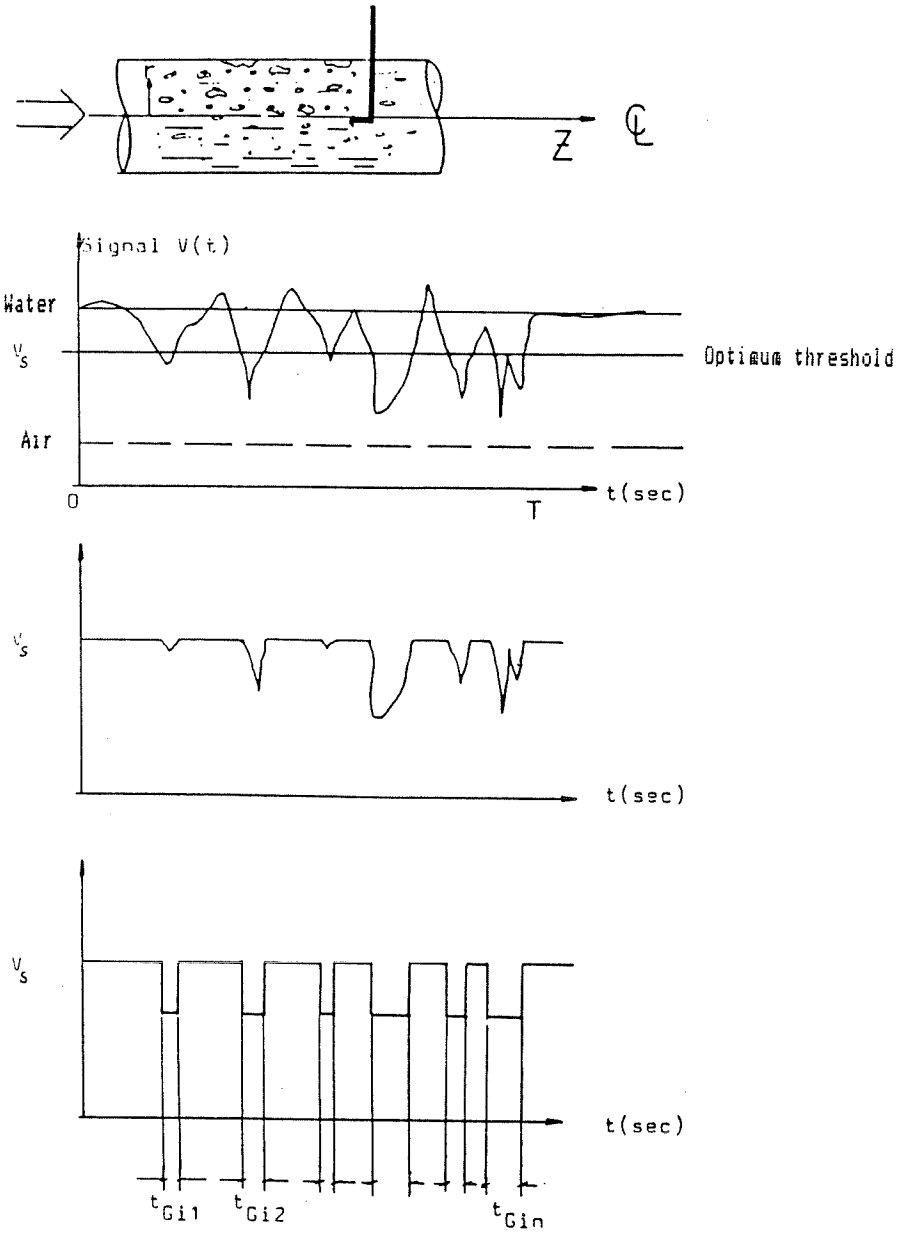

FIGURE 1: Local void fraction determined by discriminator technique with conditioned rectangular waves.

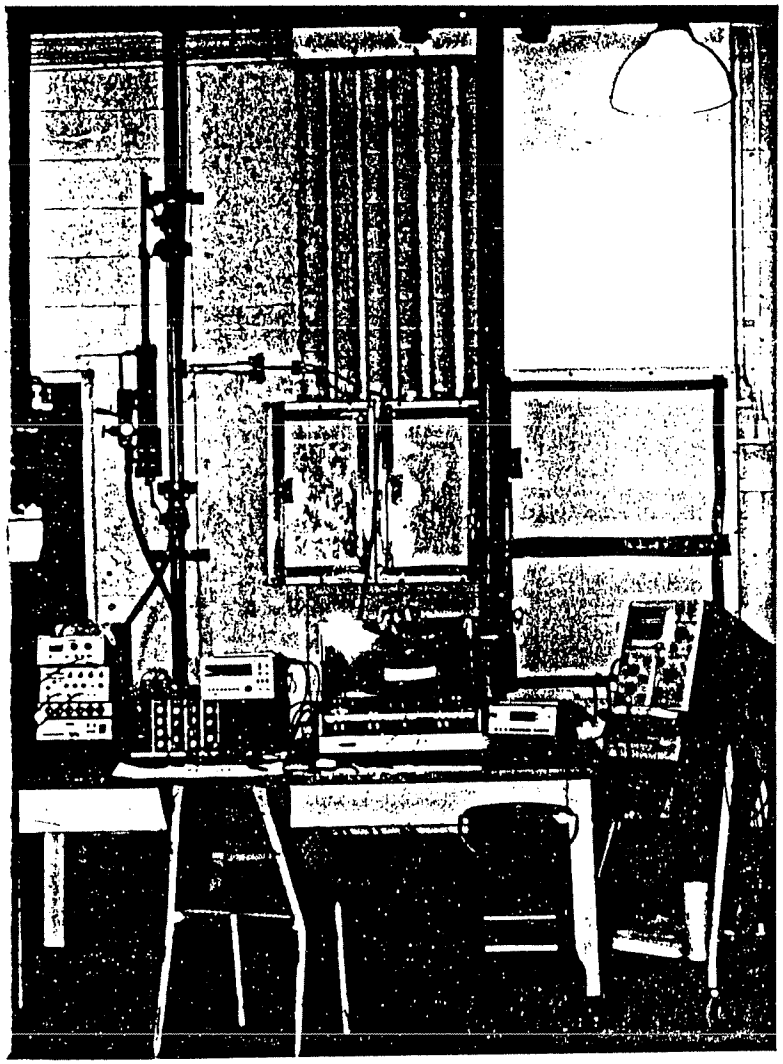

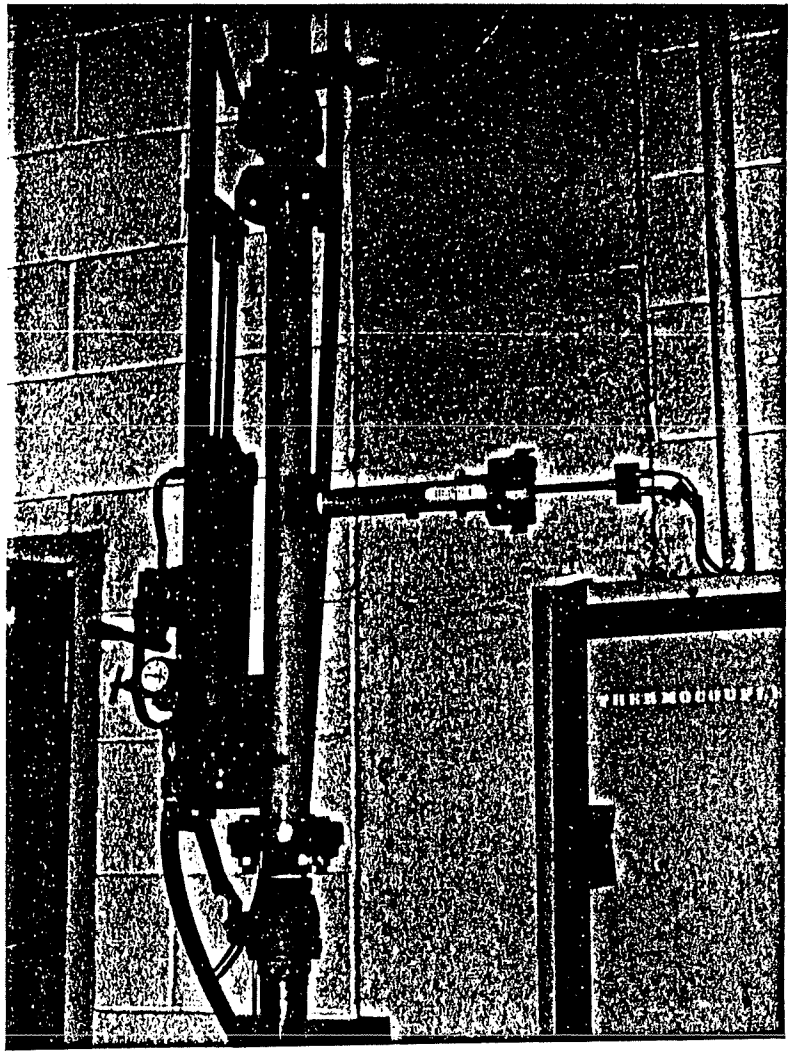

FIGURE 2: a. Vertical loop and apparatus for calibration of hot film anemometer.
b. Calibration of hot film in 2 in. pipe diameter vertical bubbly flow.

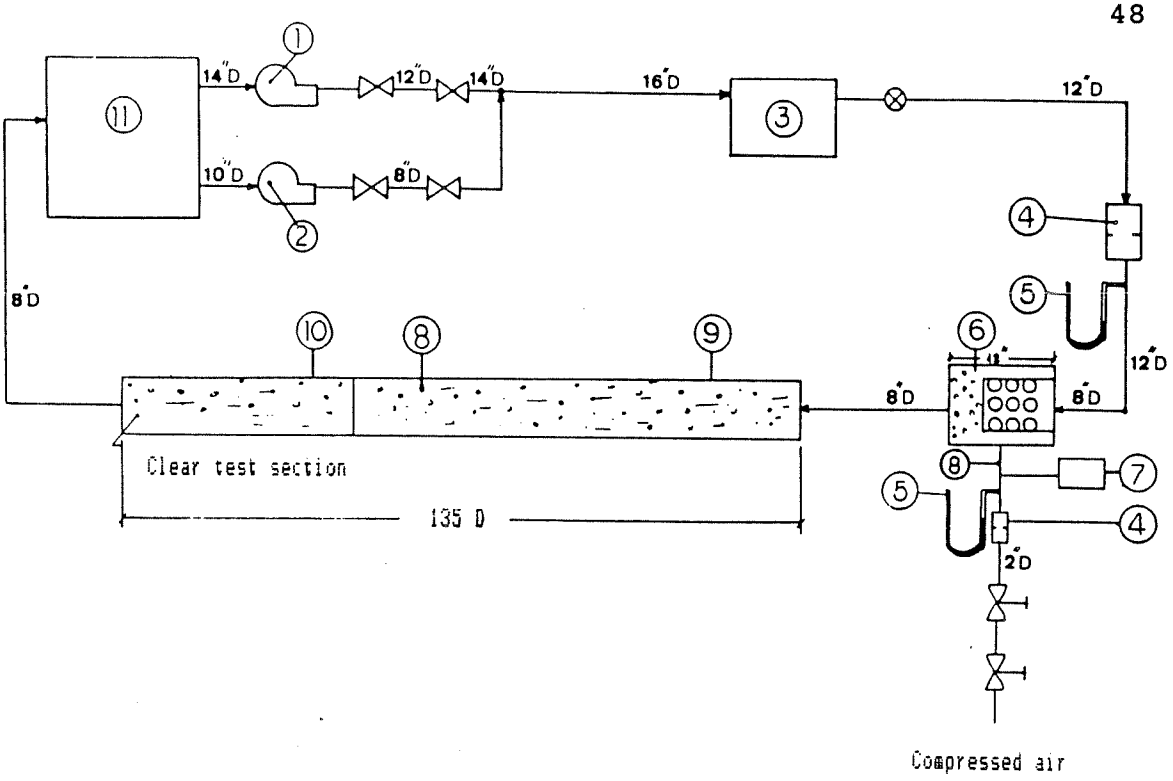

⧖ : monitoring control valve
⧖ : regulator of constant
⊗ : manual control valve

1) Pump (150 HP)
2) Pump (75 HP)
3) Closed pressure vessel (45 psi)
4) Orifice meter
5) Hg U-manometer
6) Air-Water mixer
7) Pressure gauge
8) Thermometer
9) Test section
10) Measurement apparatus (Pitot,probe)
11) Open reservoir tank

FIGURE 3: Horizontal test loop

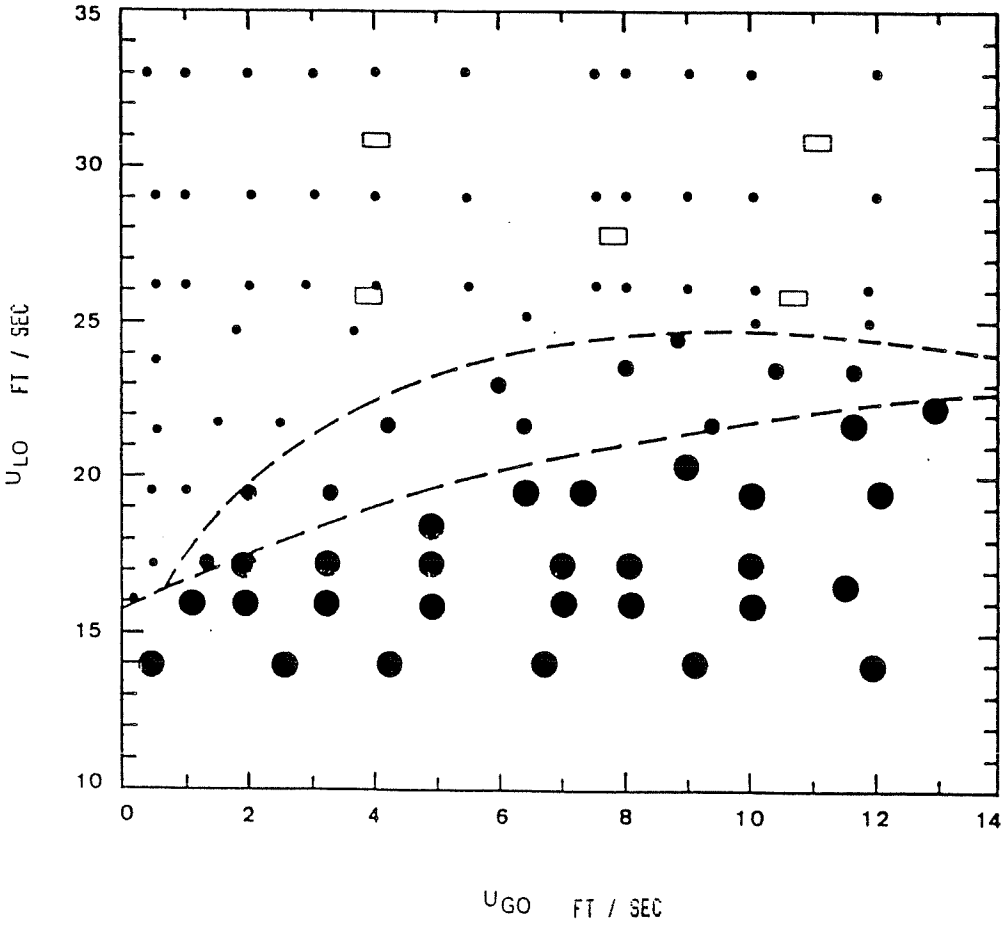

FIGURE 4: Flow map of horizontal air-water flow

(8 in. nominal diameter, fully developed flow z/D = 130)

- ● Slug flow
- ◒ Dispersed slug waved flow
- • Stratified - dispersed bubbles flow
- ▭ Values choosen for experimentation
- --- Transition zones.

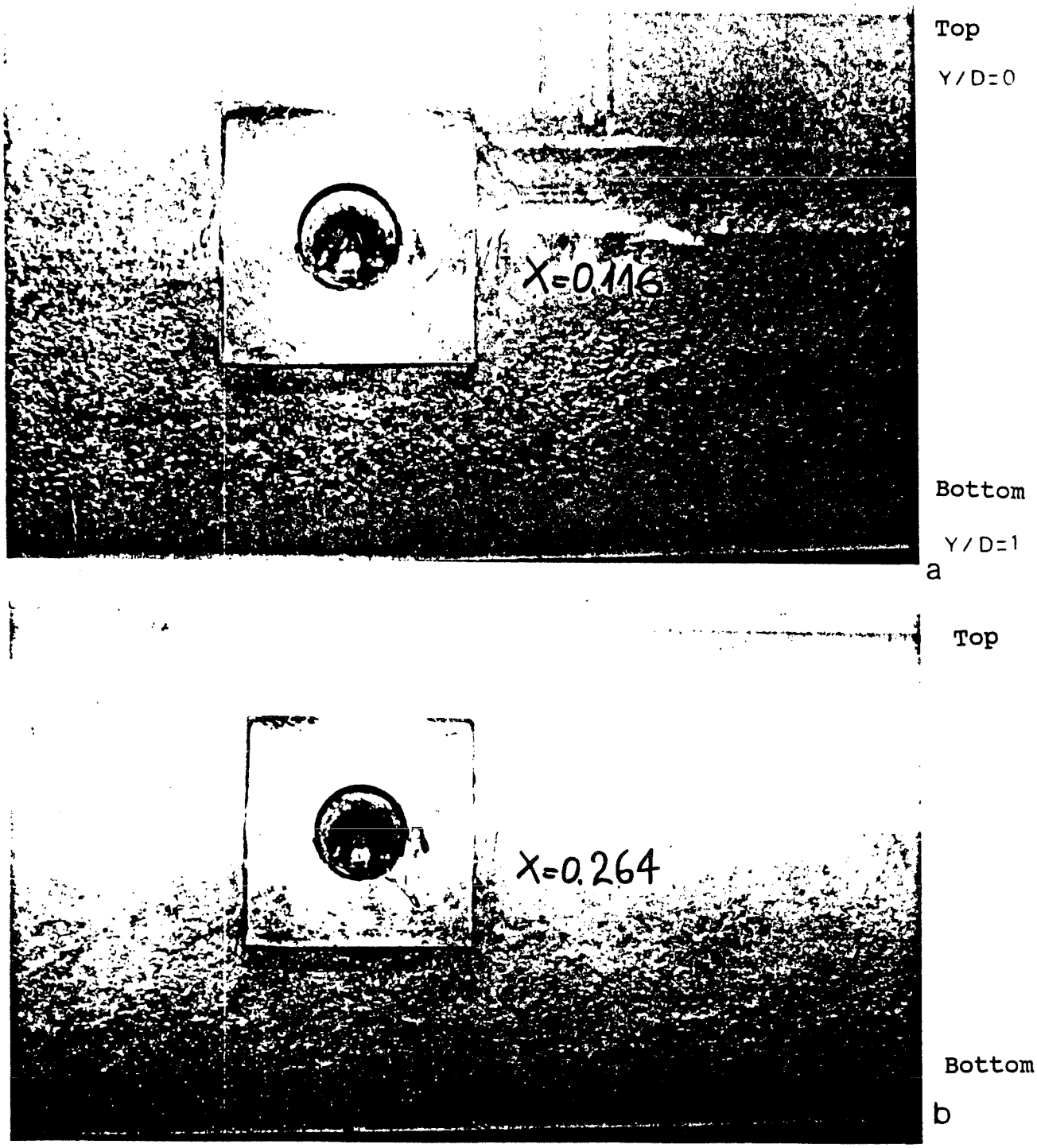

FIGURE 5: Visual observation of flow regimes in large pipe (air-water flow, horizontal, D = 8 in., elevation plane)

a. X_o = 0.116 (U_{lo} = 31.10 ft/sec)
b. X_o = 0.264 (U_{lo} = 31.10 ft/sec)
c. X_o = 0.219 (U_{lo} = 29.20 ft/sec)
d. X_o = 0.131 (U_{lo} = 26.78 ft/sec)
e. X_o = 0.292 (U_{lo} = 26.78 ft/sec)

Top

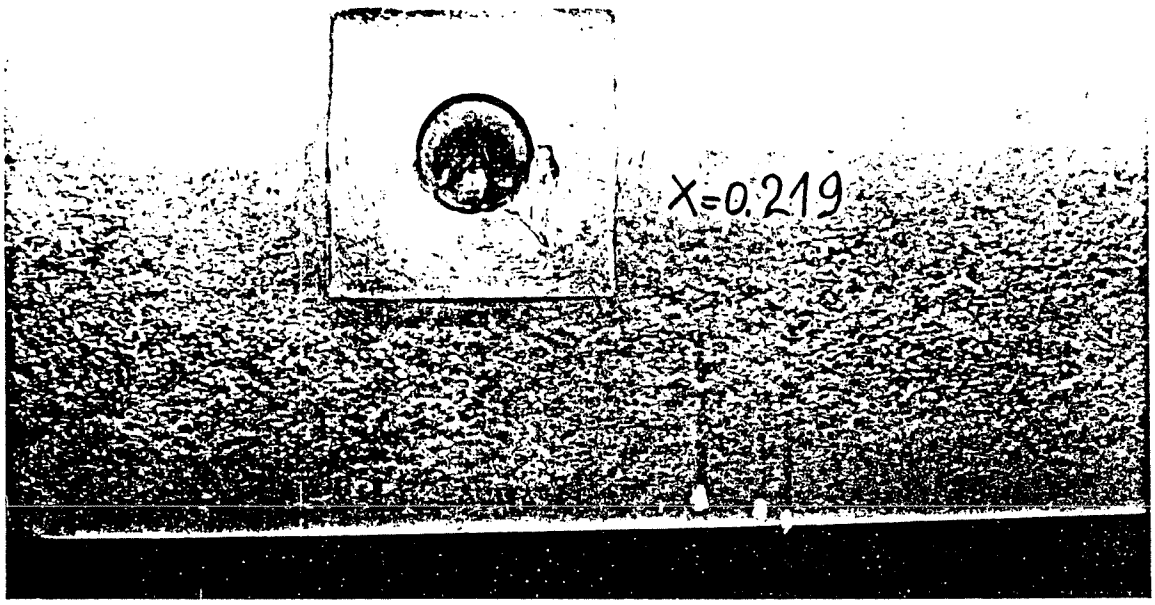

Bottom

C

Top

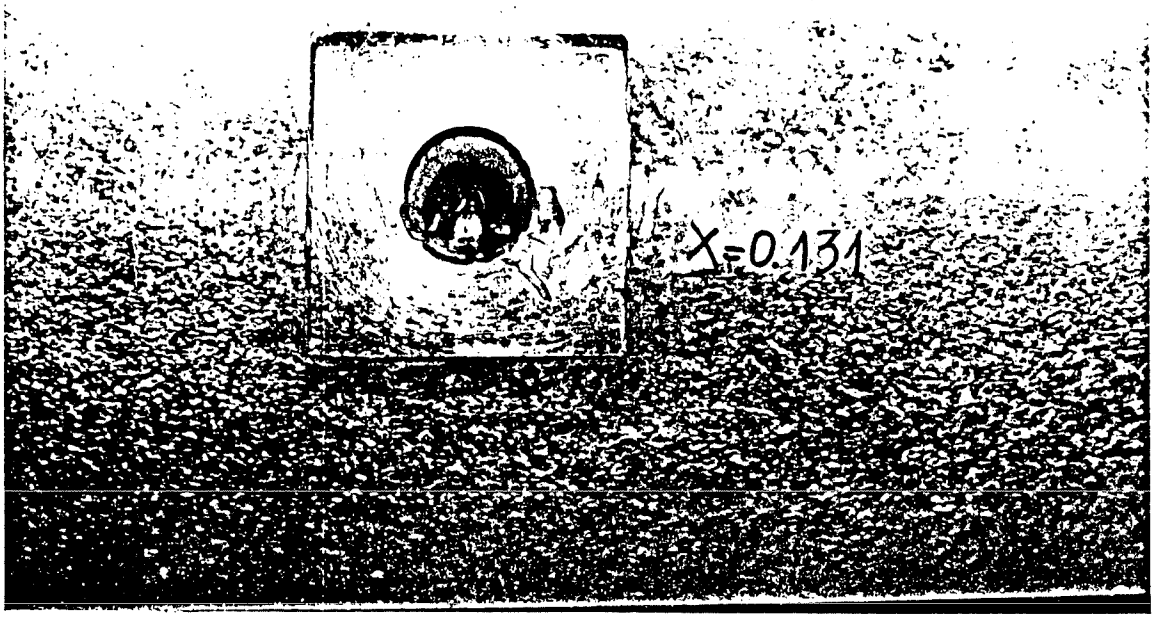

Bottom

d

Top

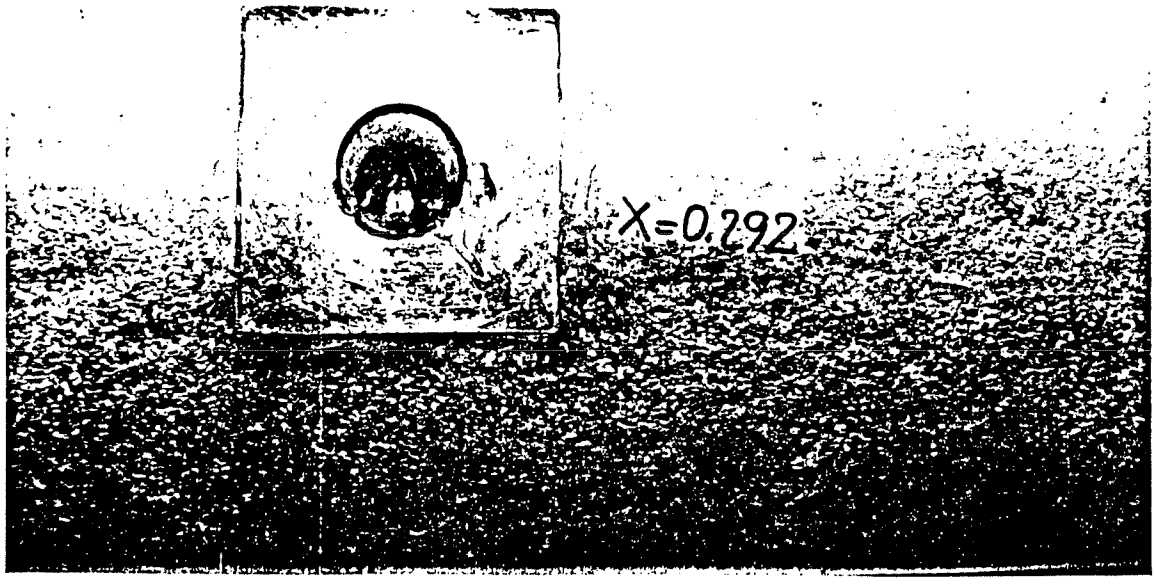

e

Bottom

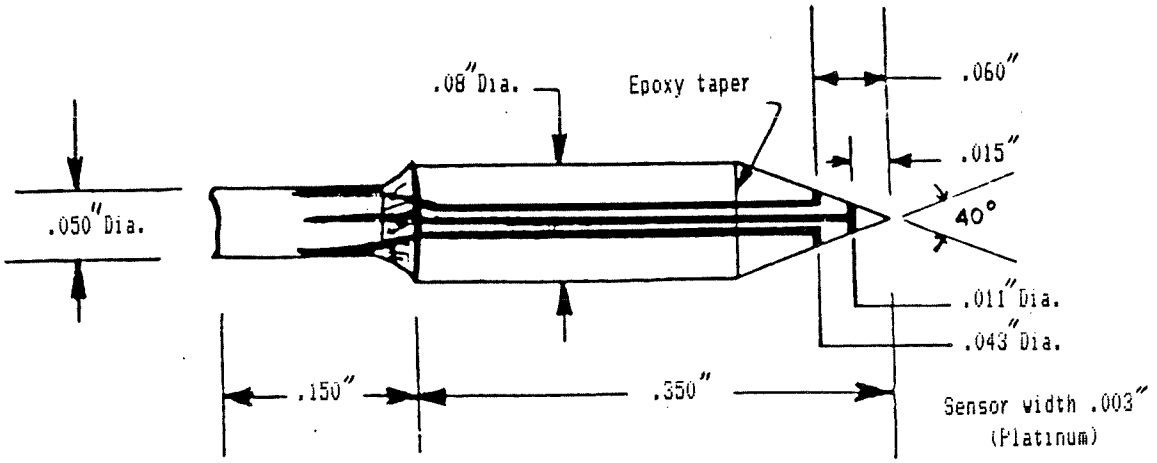

a

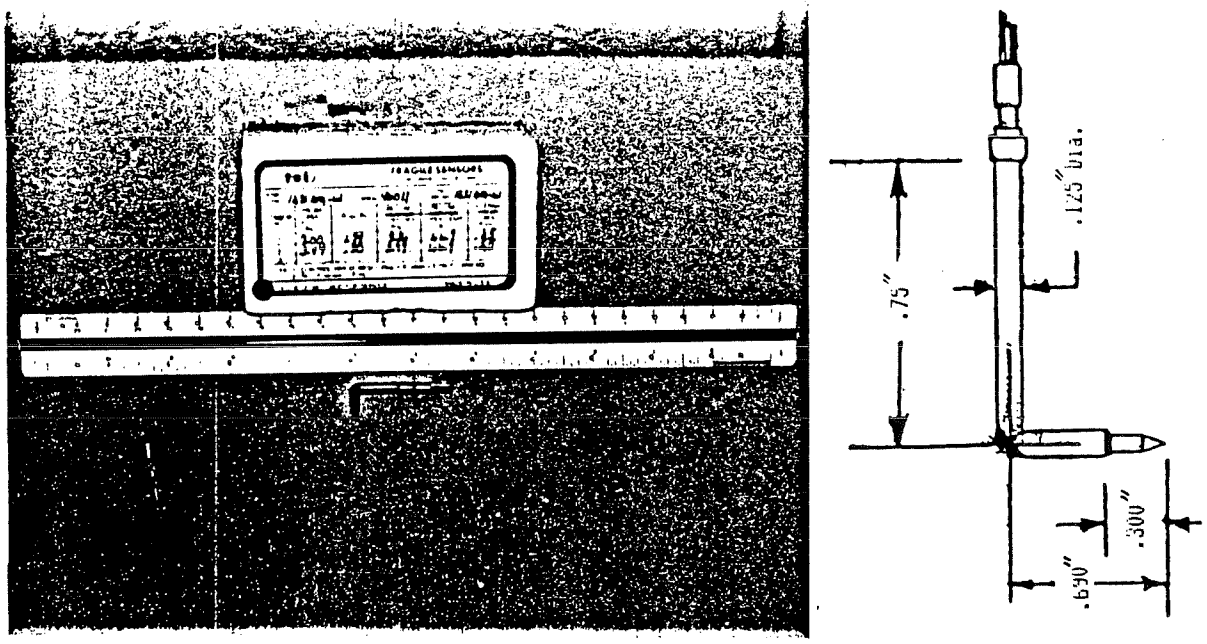

b

FIGURE 6: Double conical hot film
a. Model TSI 1231 AF-W (separate distance = 1.14 mm)
b. Model TSI 1231 AM-W (separate distance = 3.30 mm)

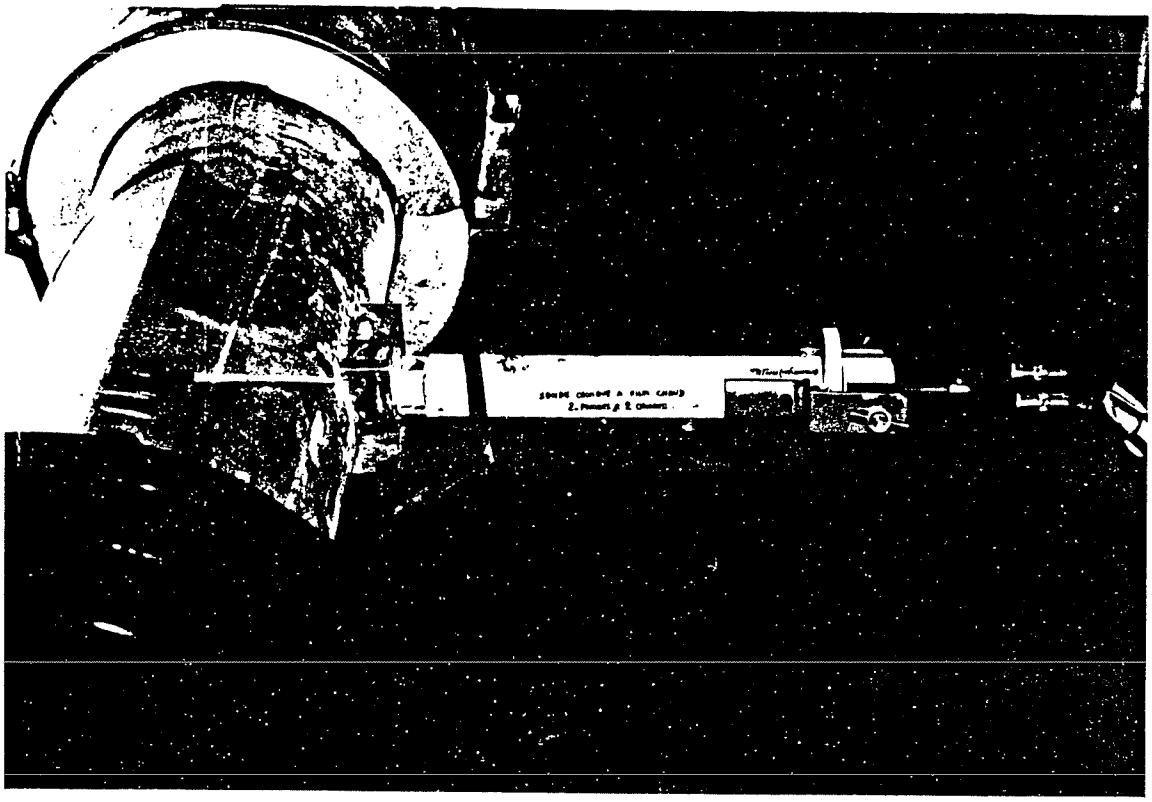

FIGURE 7: Measurement of void fraction and bubble velocity with double conical hot film in radial plane

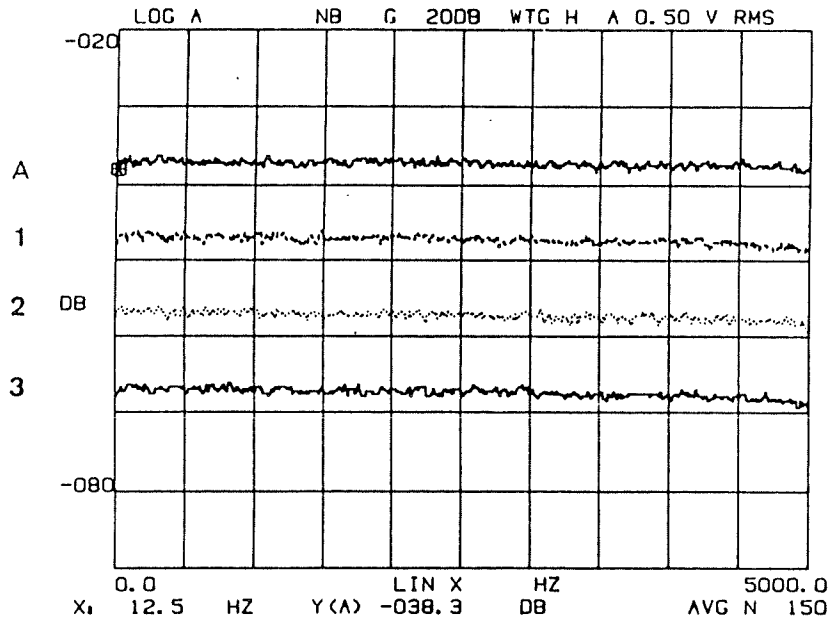

a

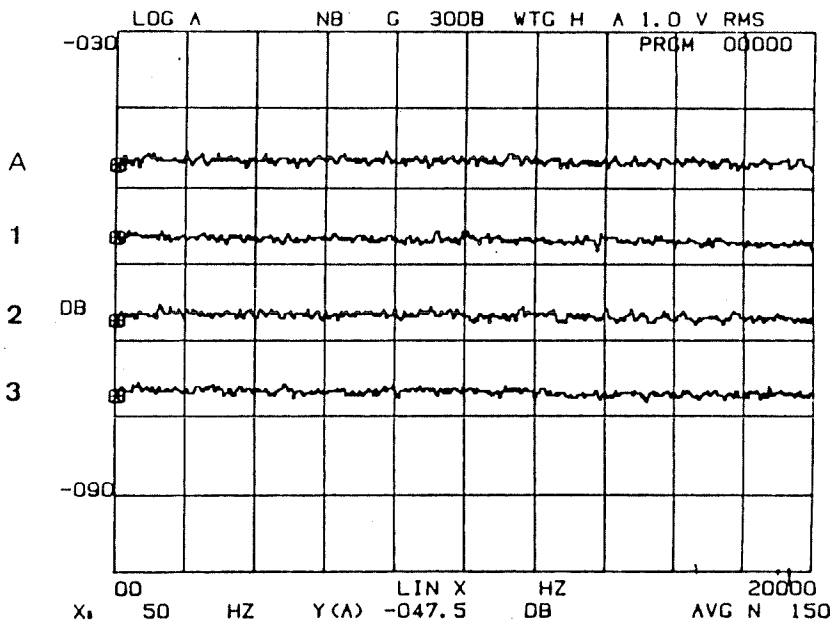

b c

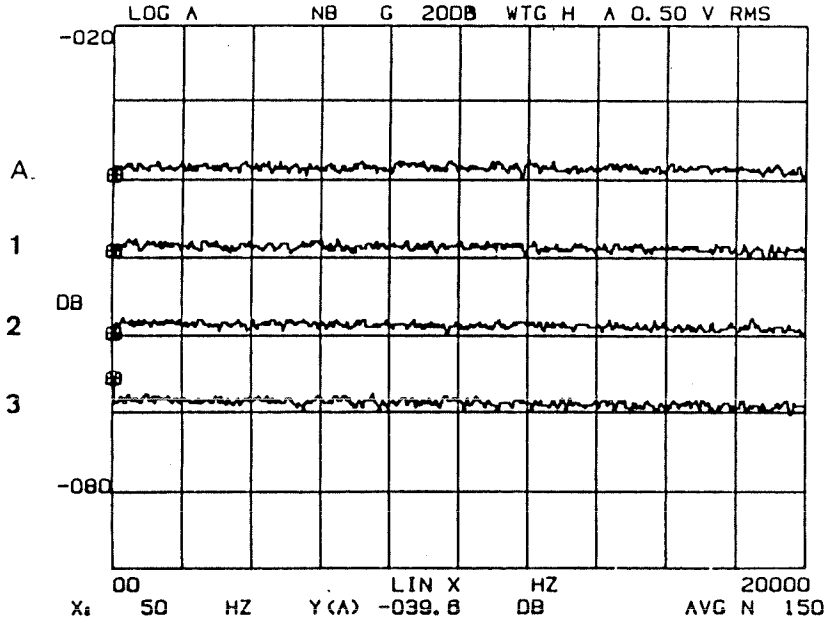

FIGURE 8:

Calibration of magnetic recorder Racal 4 DS with the digital analyzer SD 375.

A: input signal.

1,2,3: output siganls of channel 1, 2 and 3.

a) Tape speed: 15 in/s (53 mV)

b) Tape speed: 30 in/s (27 mV)

c) Tape speed: 60 in/s (21 mV)

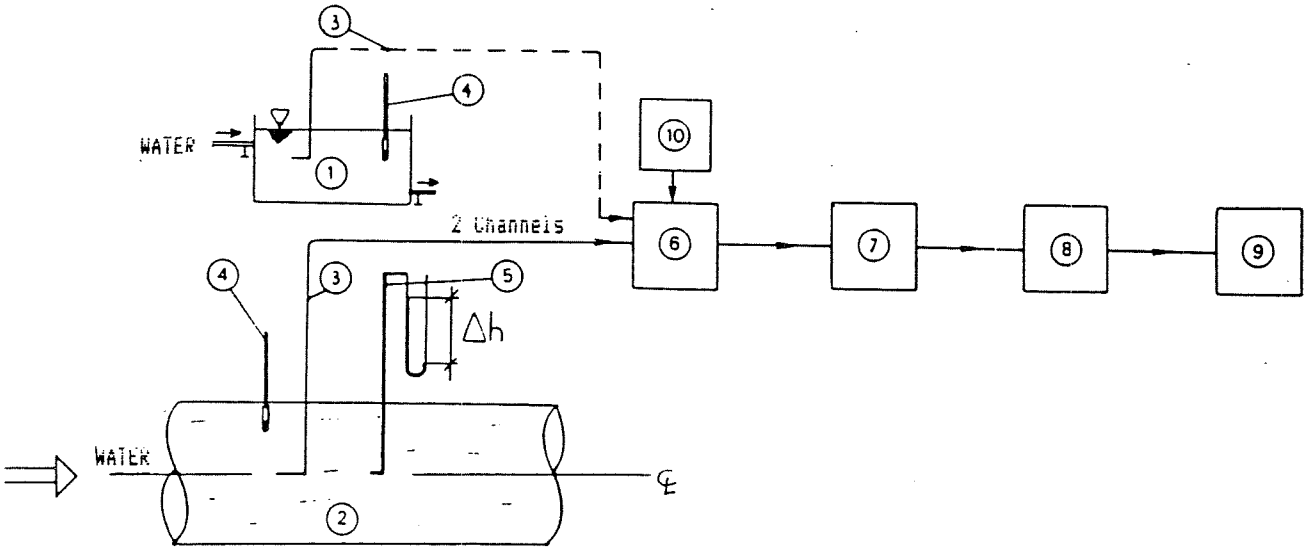

1) container ($U_L \simeq 0$)
2) Clear pipe (8 dia., z/D = 130, U 0)
3) Hot film anemometers (TSI 1231 AF-W and 1231 AM-W)
4) Thermometer
5) Pitot tube (regular Pitot 88S250J or Average Flobar 1350L)
6) 2 constant temperature anemometers DISA 55D01
7) Filters and amplifiers (ITHACO, Amp. 45, filt. 4113)
8) Oscilloscope TEKTRONIK
9) Voltmeters TSI 1076
10) Frequency generator

FIGURE 9: Calibration of hot film in water flow

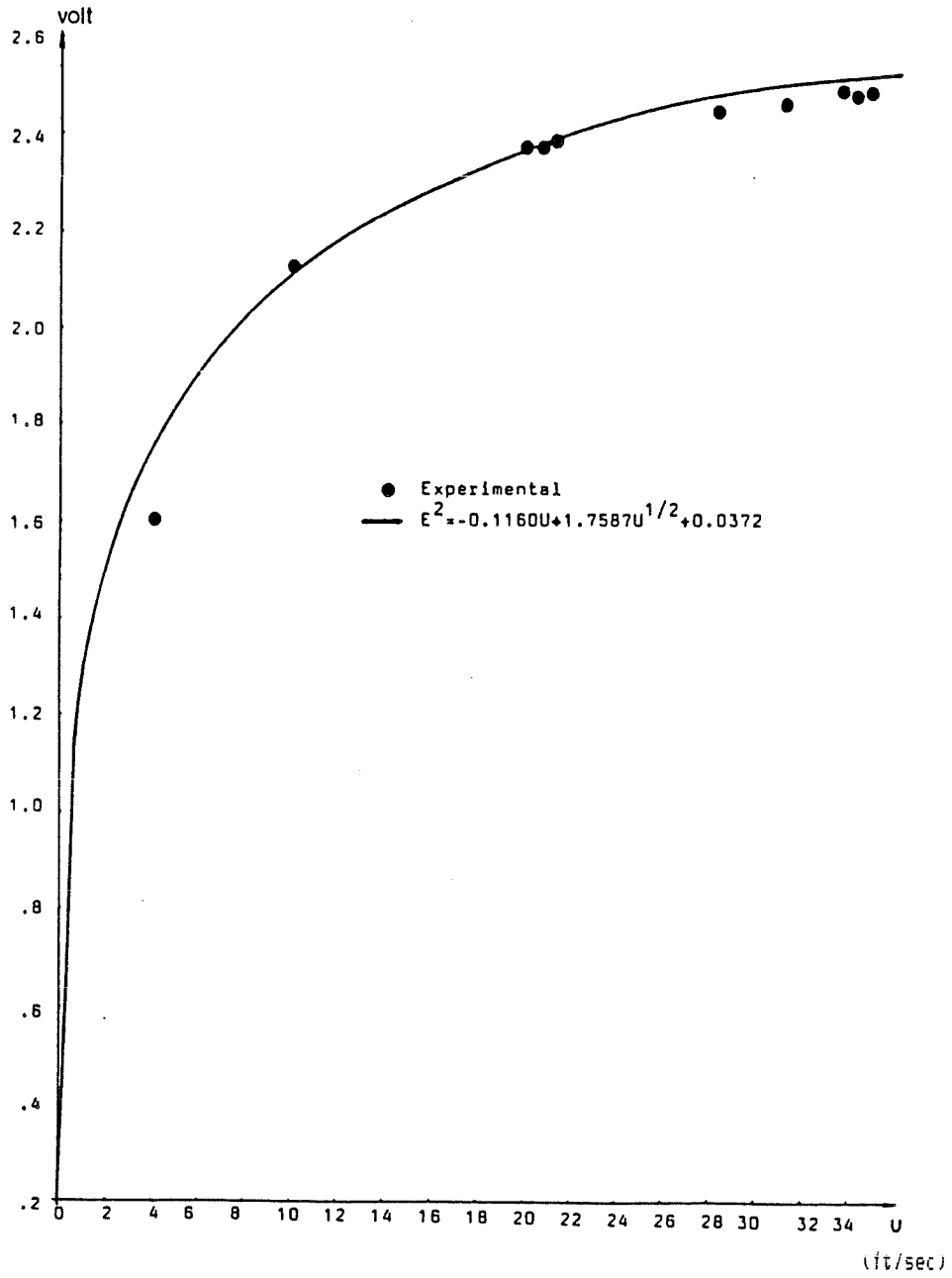

FIGURE 10: Calibration curve of the hot film 1231 AF-W (front sensor)

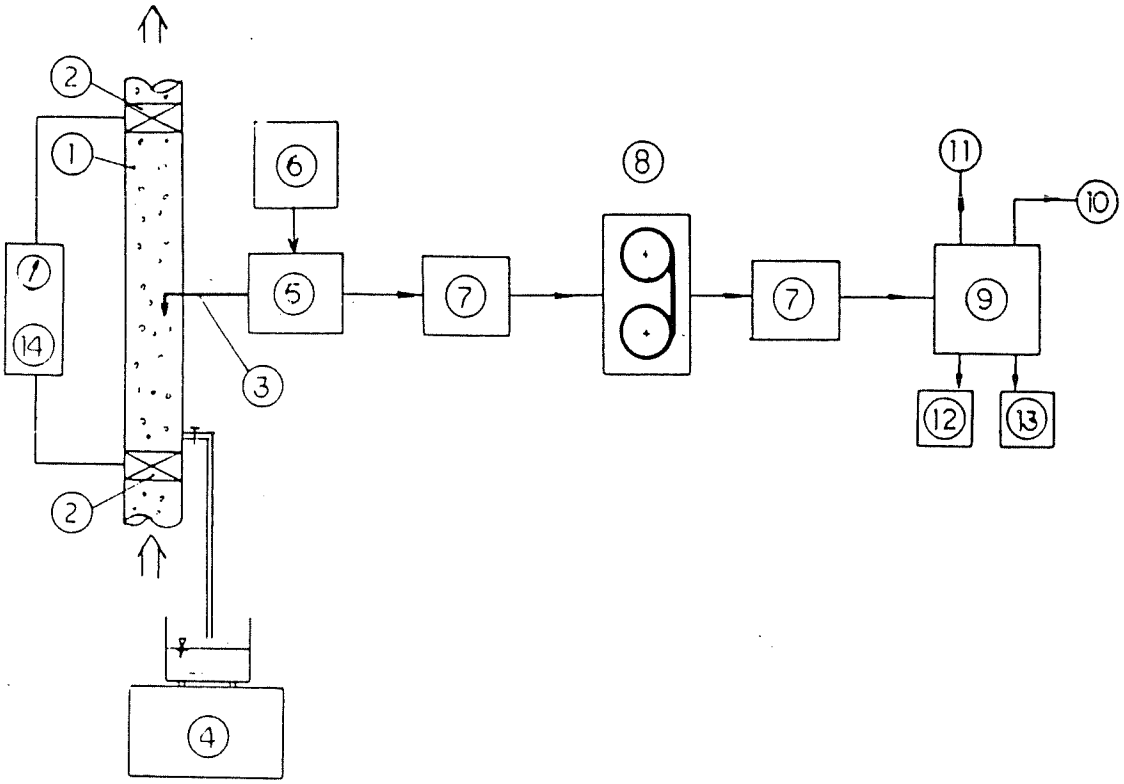

1) Vertical clear pipe, calibration section (2 ID, z/D = 42)
2) Quick closing valves (2 ID)
3) Double conical hot film probe (TSI 1231 AM-W, ser. 46011)
4) Digital scale (SARTORINS 1303 MP)
5) Constant temperature anemometer (DISA 55D01)
6) Power supply (30 V, SORENSEN QRD 30-1)
7) Filters and amplifiers (ITHACO, AMP. 451, Filt.4113)
8) Portable magnetic recorder (RACAL 4DS)
9) Discriminator circuit of adjustable threshold (POLY SC2)
10) Memorised oscilloscope (TEKTRONIC, 561A)
11) Voltmeter (TRUE RMS VOLTMETER TSI 1076)
12) Time counter (UNIVERSAL COUNTER RACAL 835)
13) Frequency meter (DAWE FREQ METER)
14) High pressure speed control box (max. 90 psig, nor 60-70 psig)

FIGURE 11: Schematic diagram of calibration of hot film in air-water flow

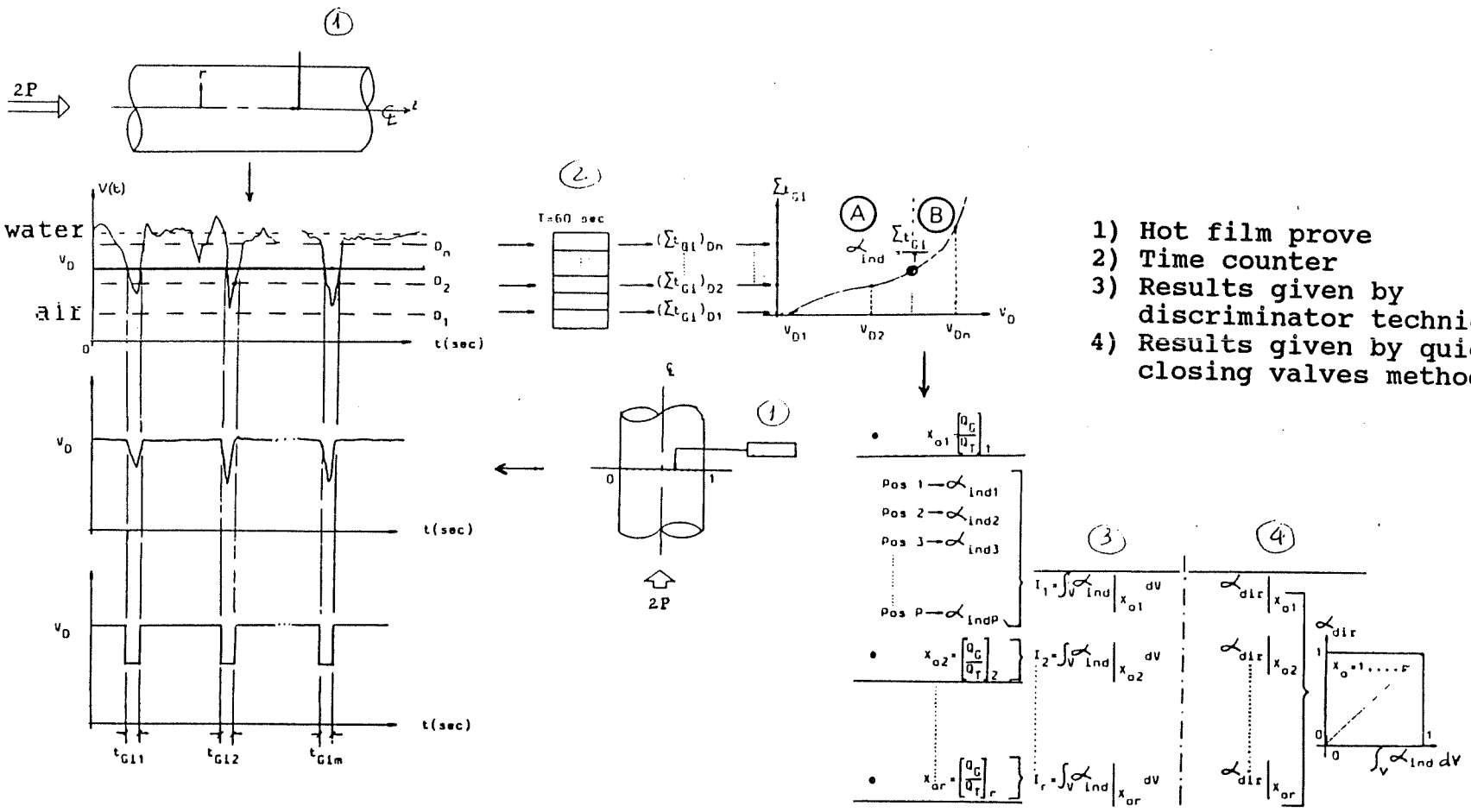

FIGURE 12: Calibration procedure of hot film for determining void fraction

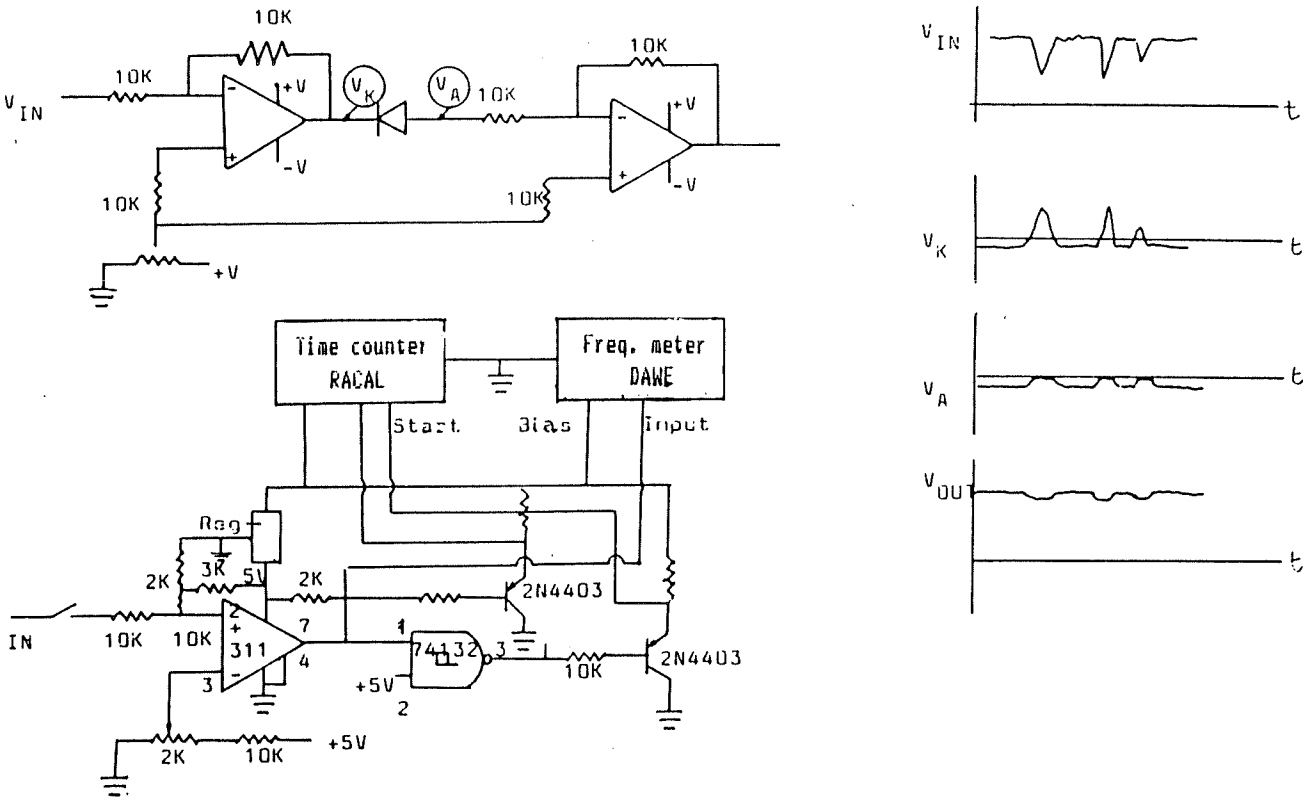

FIGURE 13: Discriminator circuit

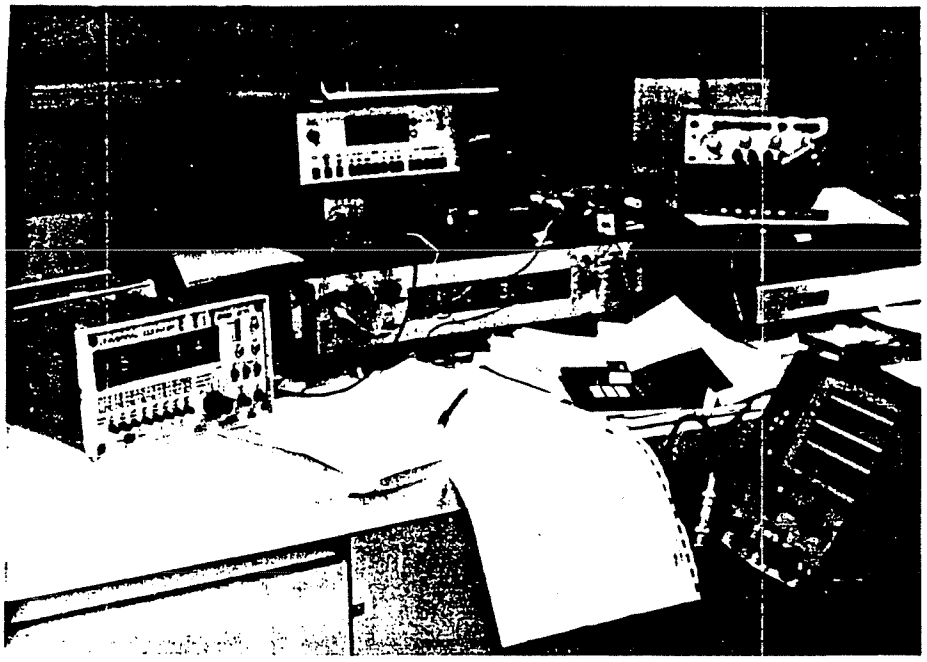

a

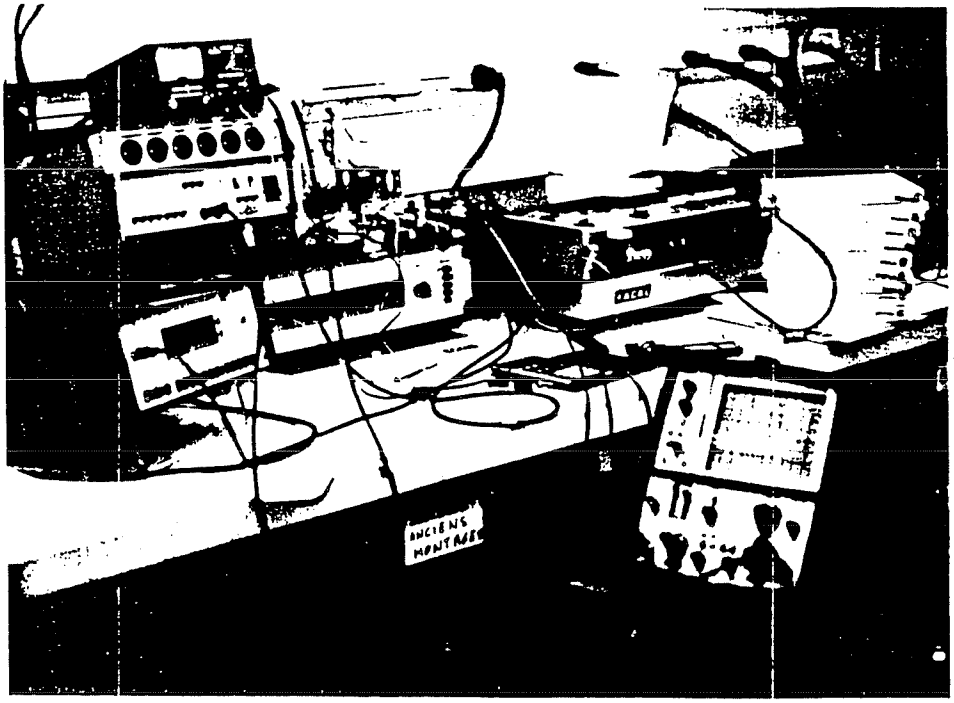

b

FIGURE 14:

Electronic equipment determining void fraction
a. Control of electric circuit with rectangular and/or sinusoidal waves.
b. Determination of void fraction and bubble passing frequency

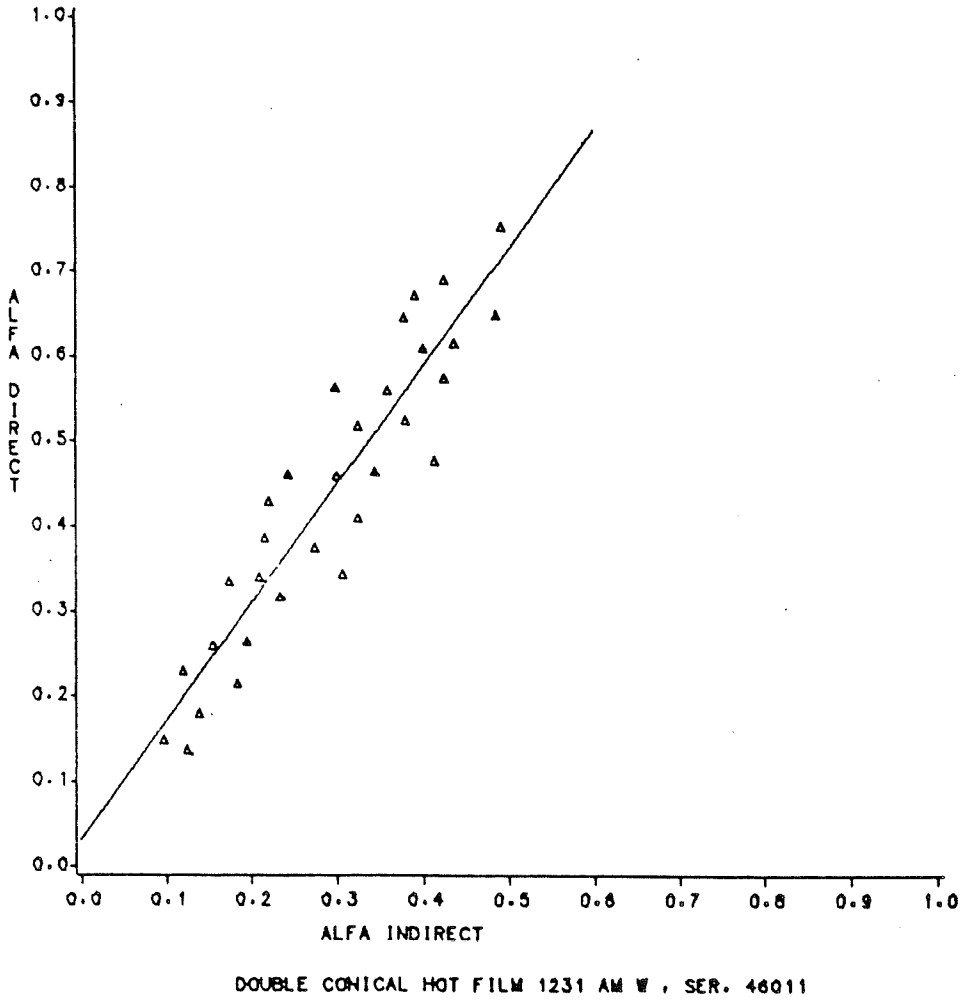

FIGURE 15: Calibration curve for void fraction (void by quick closing valves = 1.426 * void by hot film)

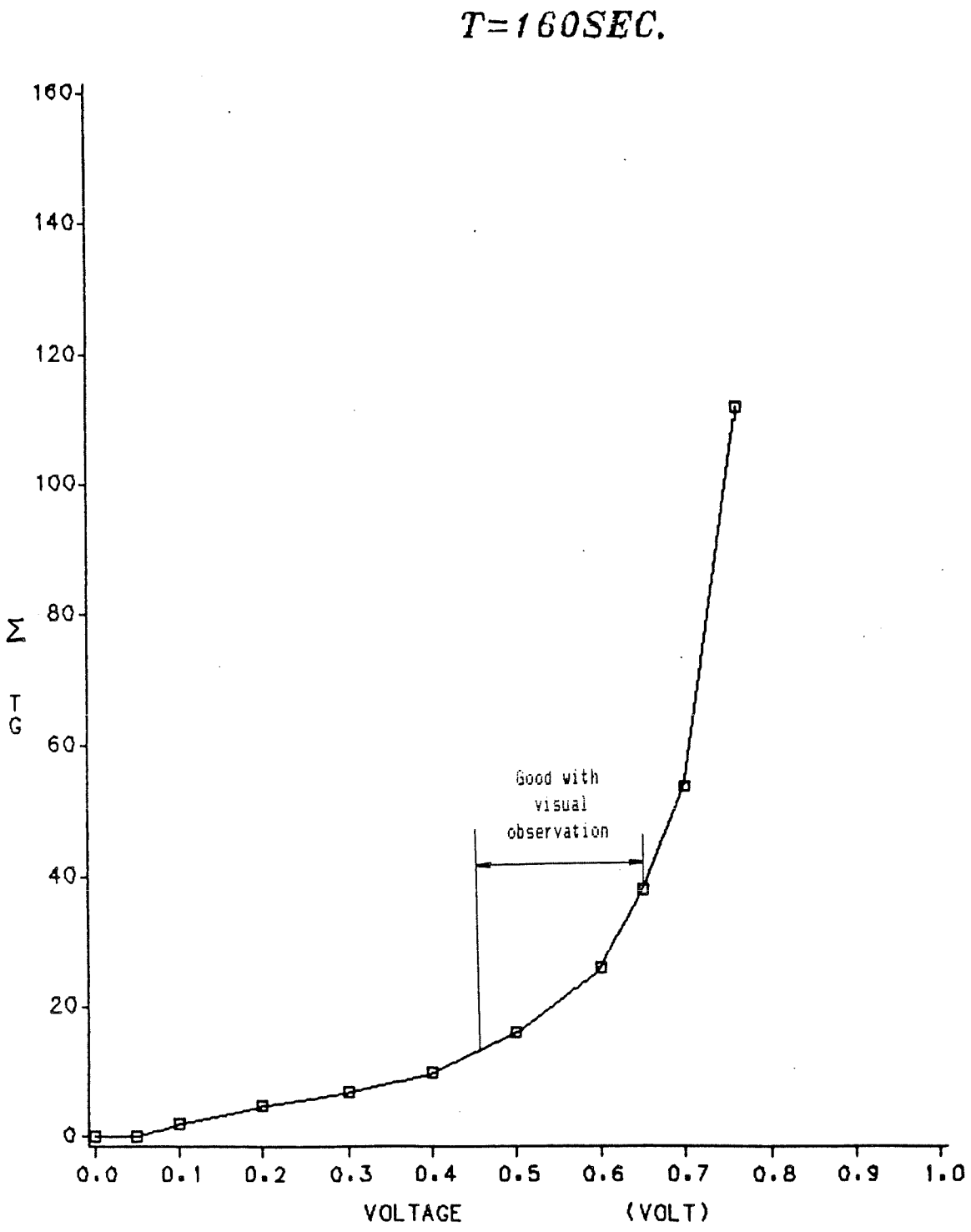

FIGURE 16:

Illustration of void fraction determination with optimum threshold (z/D = 74, y/D = 0.5, X = 0.219, @ 0.610 V DC, void = 0.163)

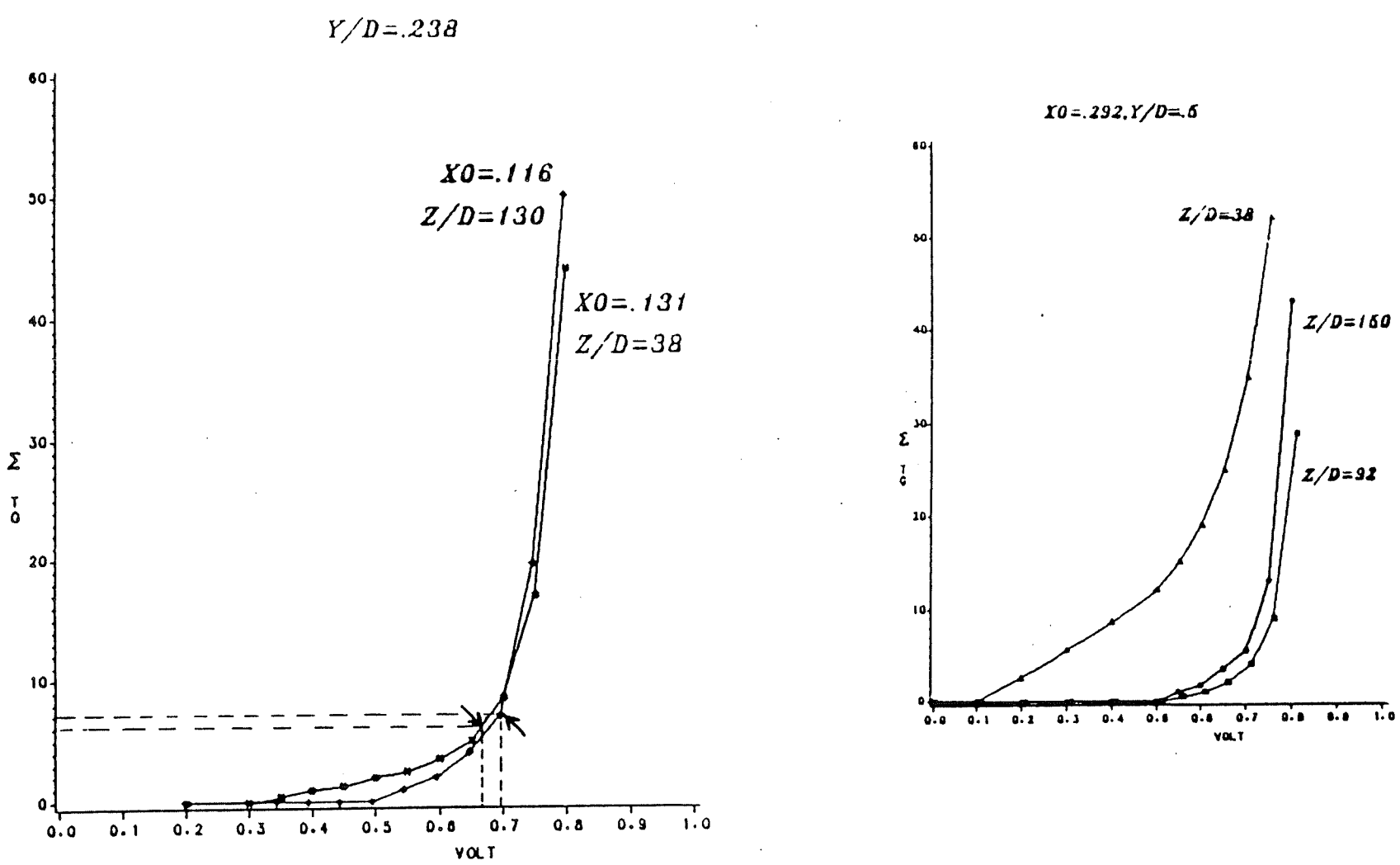

FIGURE 17: Average duration of bubbles obtained at optimum value of threshold level, optimum void = $\Sigma t_G/T$ (front sensor).

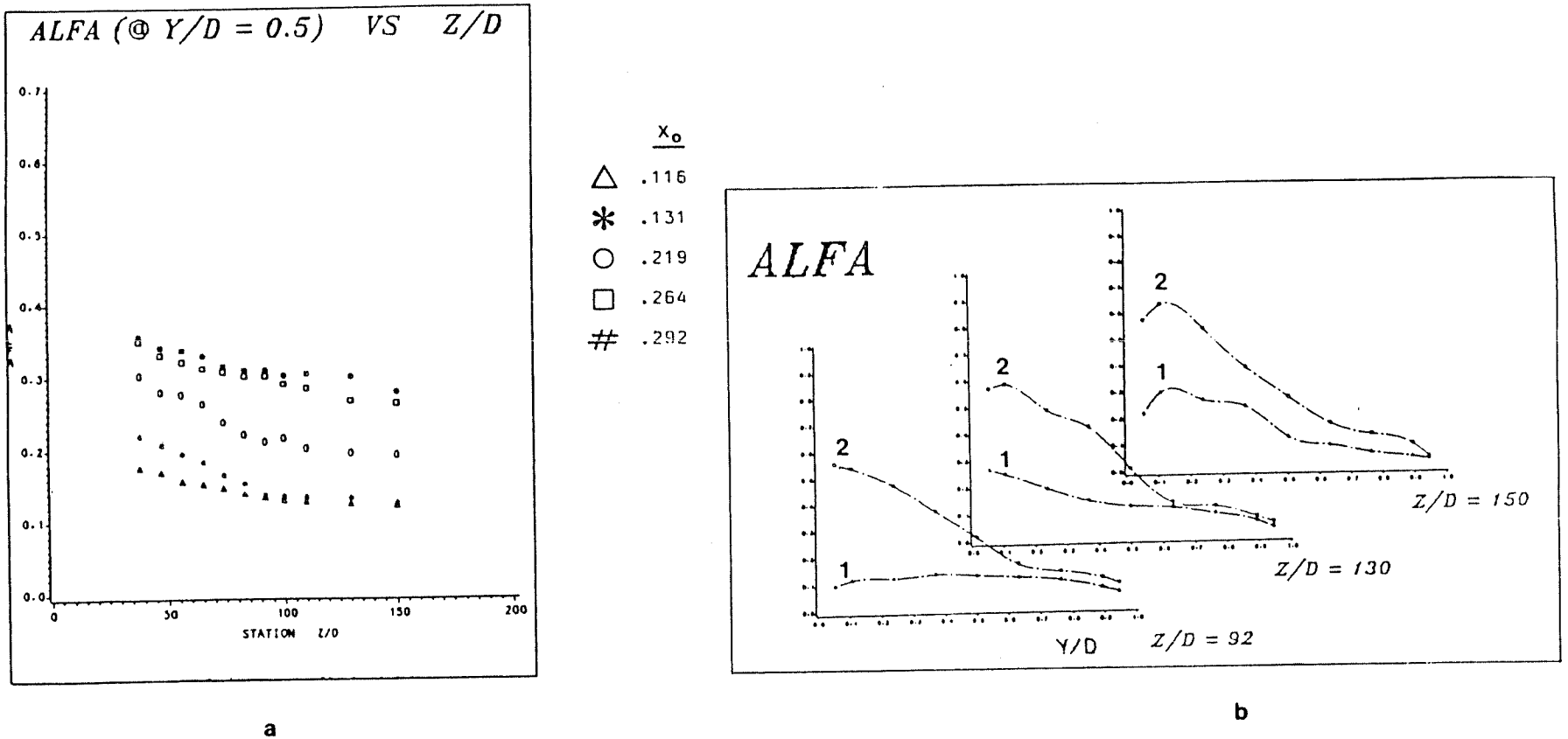

a

b

FIGURE 18:

Longitudinal distribution of void fraction for different flow volumetric quality, X_o:
a. Void fraction measured at pipe centre line
b. Void fraction profiles in tranversal plane of fully developed flow ($Q_{l\,o}$ = 4373 USGPM, 1 : X = 0.116, 2: X = 0.264)

$$\frac{\alpha_{CL}}{\alpha_{FD}} = (0.015\ Xo - 0.0093)(Z/D) - 1.88Xo + 2.03$$

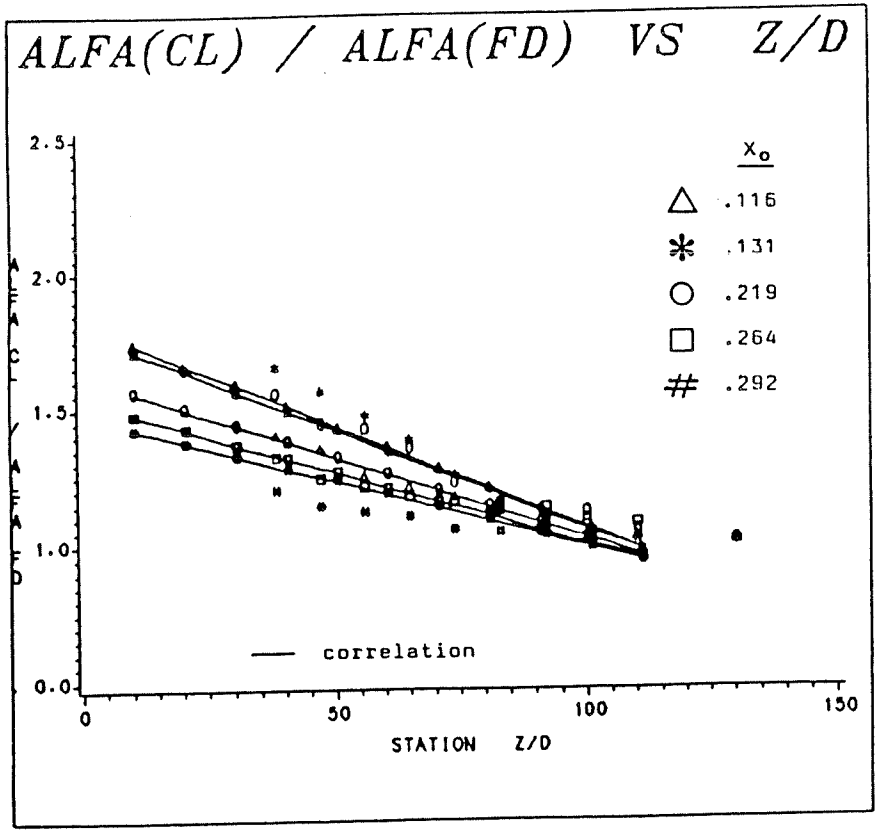

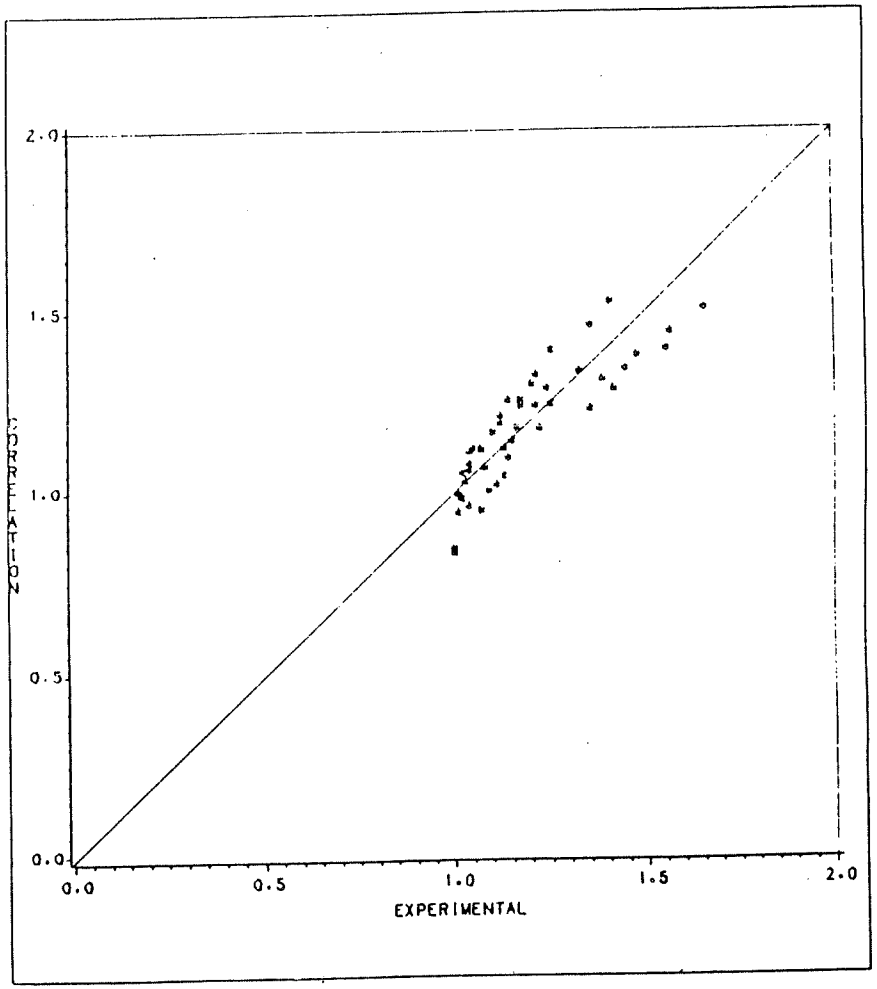

FIGURE 19: Longitudinal distribution of void centre line / void fully developed flow

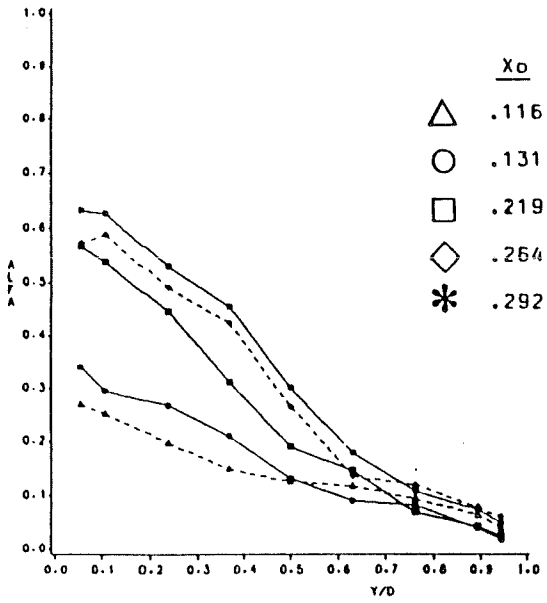

a

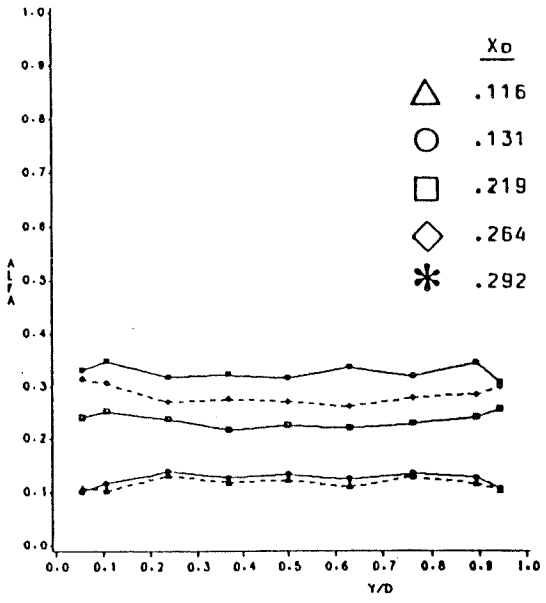

b

FIGURE 20: a. Void fraction profiles in transversal plane
b. Void fraction profiles in radial plane

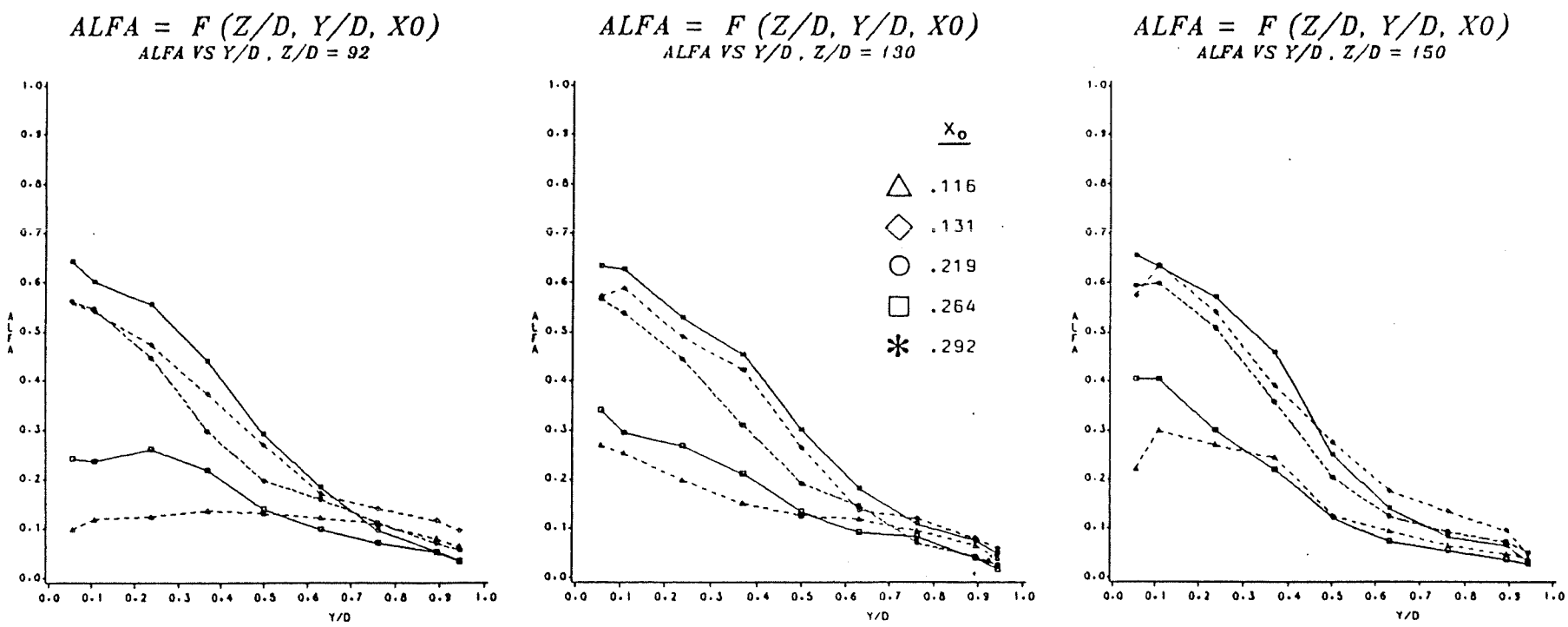

FIGURES 21: a. Variation of void fraction profiles in terms of various flow volumetric qualities X, comparison made at 3 axial location.
b. Variation of void fraction profiles in terms of various axial locations z/D, comparison made for 5 values of flow volumetric quality X.
c. Variation of local void fraction in terms of radial position y/D, for various flow volumetric qualities and axial location.

ALFA = F (Z/D, Y/D, XO)

ALFA VS Y/D , XO = .116

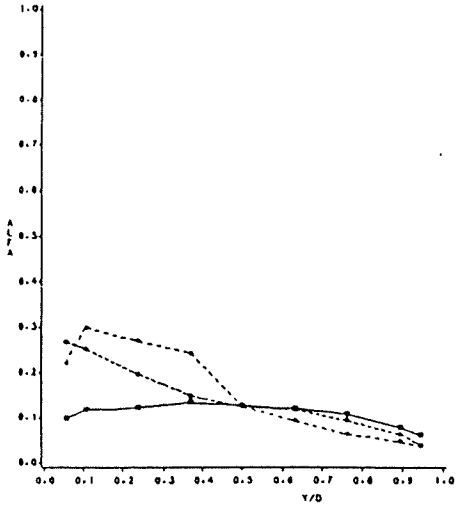

ALFA = F (Z/D, Y/D, XO)

ALFA VS Y/D , XO = .131

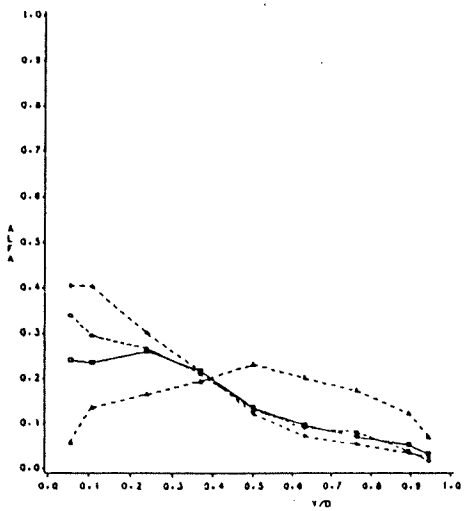

ALFA = F (Z/D, Y/D, XO)

ALFA VS Y/D , XO = .219

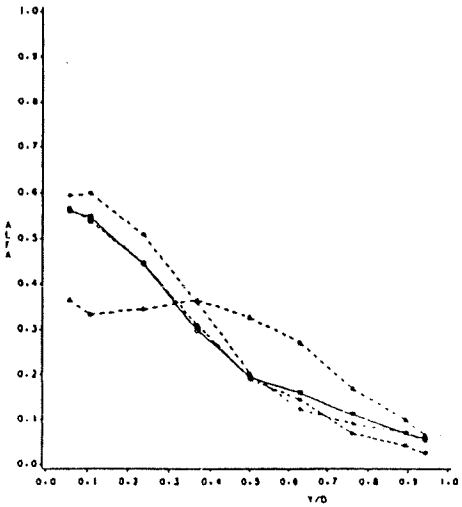

ALFA = F (Z/D, Y/D, XO)

ALFA VS Y/D , XO = .264

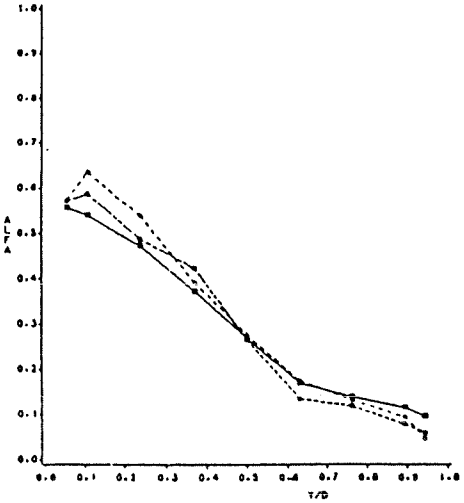

ALFA = F (Z/D, Y/D, XO)

ALFA VS Y/D , XO = .292

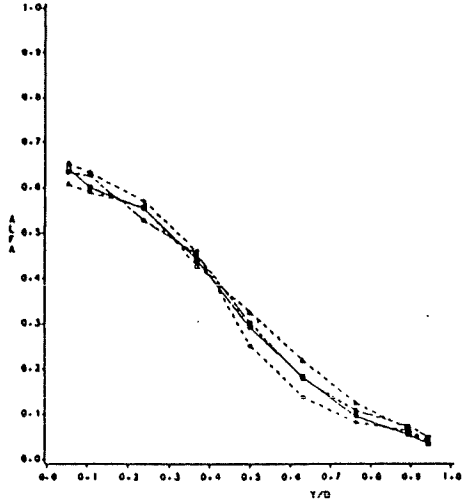

Z/D

△ 38

□ 92

○ 130

◇ 150

ALFA = F (Z/D, Y/D, XO)

ALFA VS XO , Z/D = 92

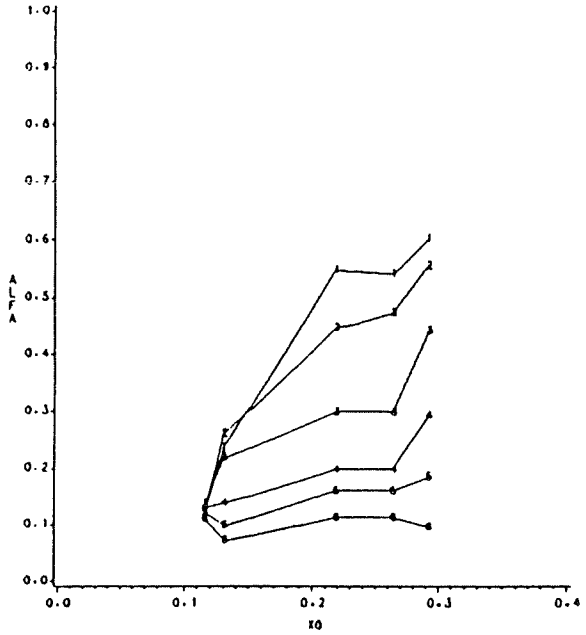

ALFA = F (Z/D, Y/D, XO)

ALFA VS XO , Z/D = 130

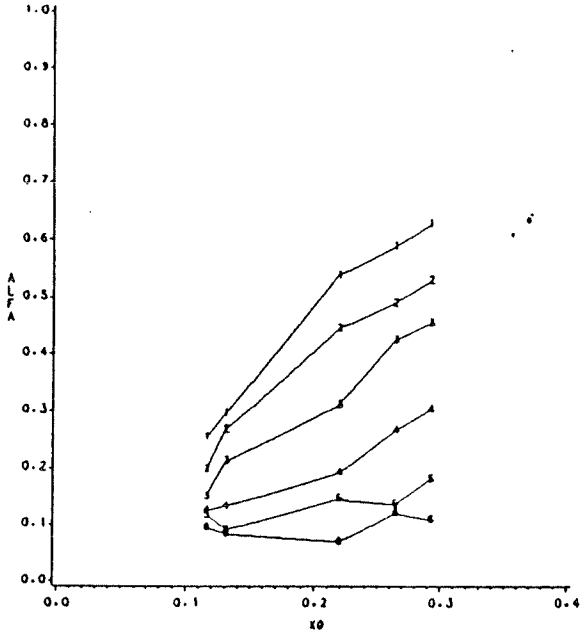

ALFA = F (Z/D, Y/D, XO)

ALFA VS XO , Z/D = 150

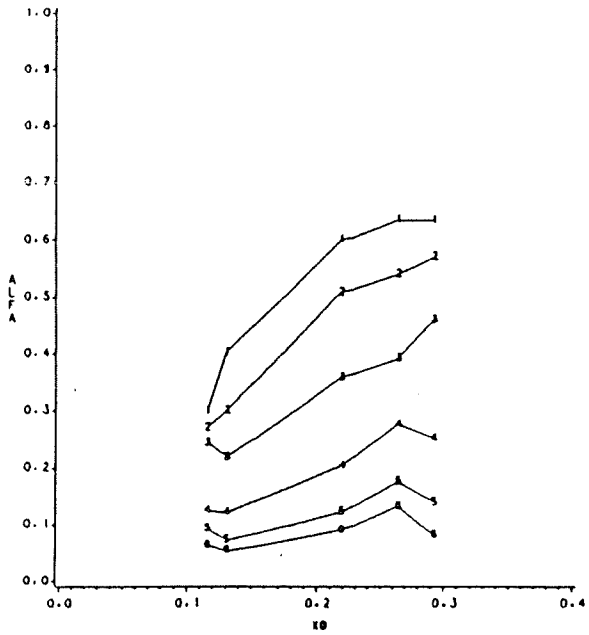

Y/D

1- 0.055
2- 0.107
3- 0.238
4- 0.364
5- 0.500
6- 0.631

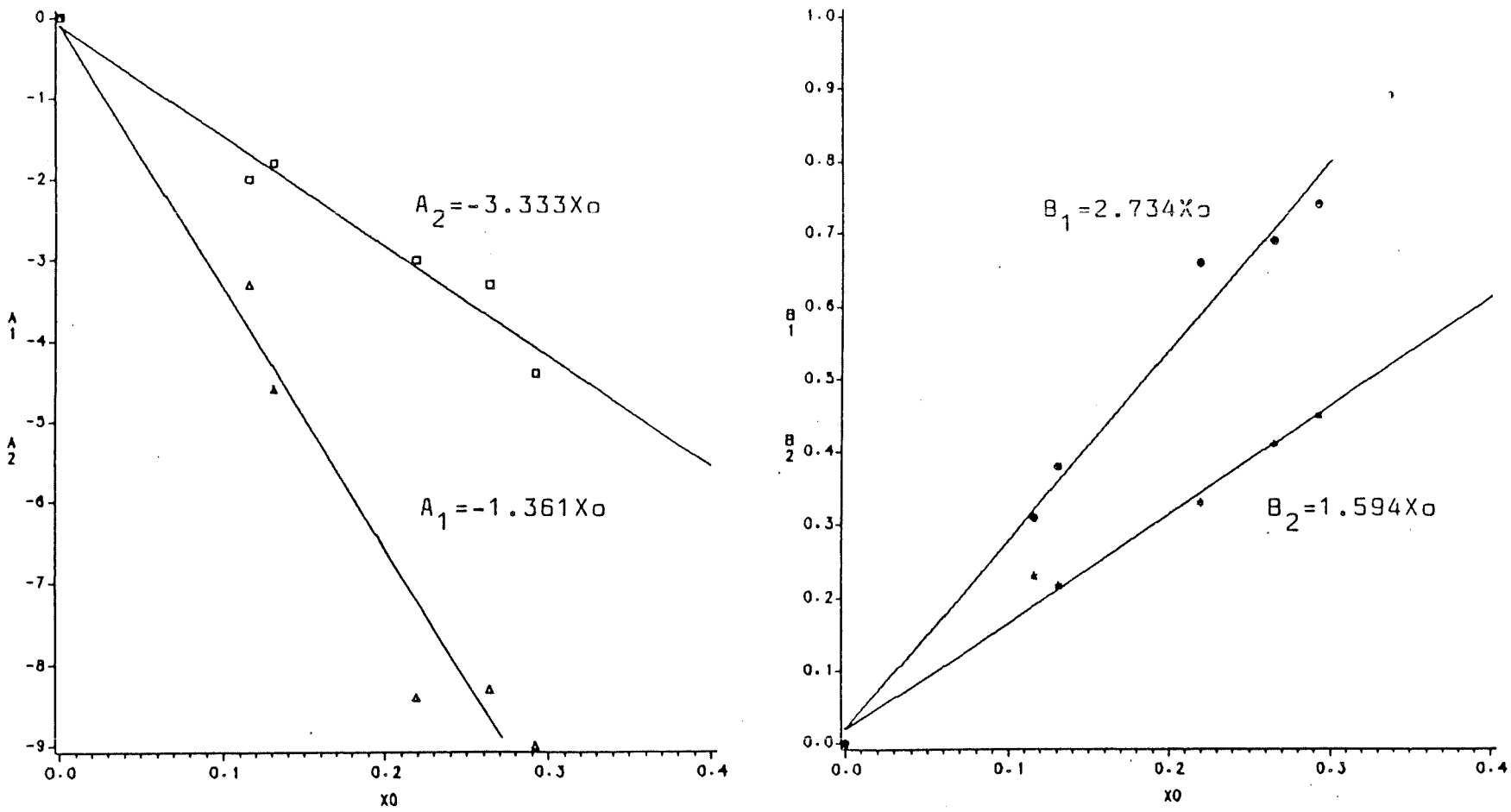

FIGURE 22:

Variation of constants A_1 , B_1 , A_2 and B_2 in linear model of void fraction in terms of flow volumetric quality X_o .

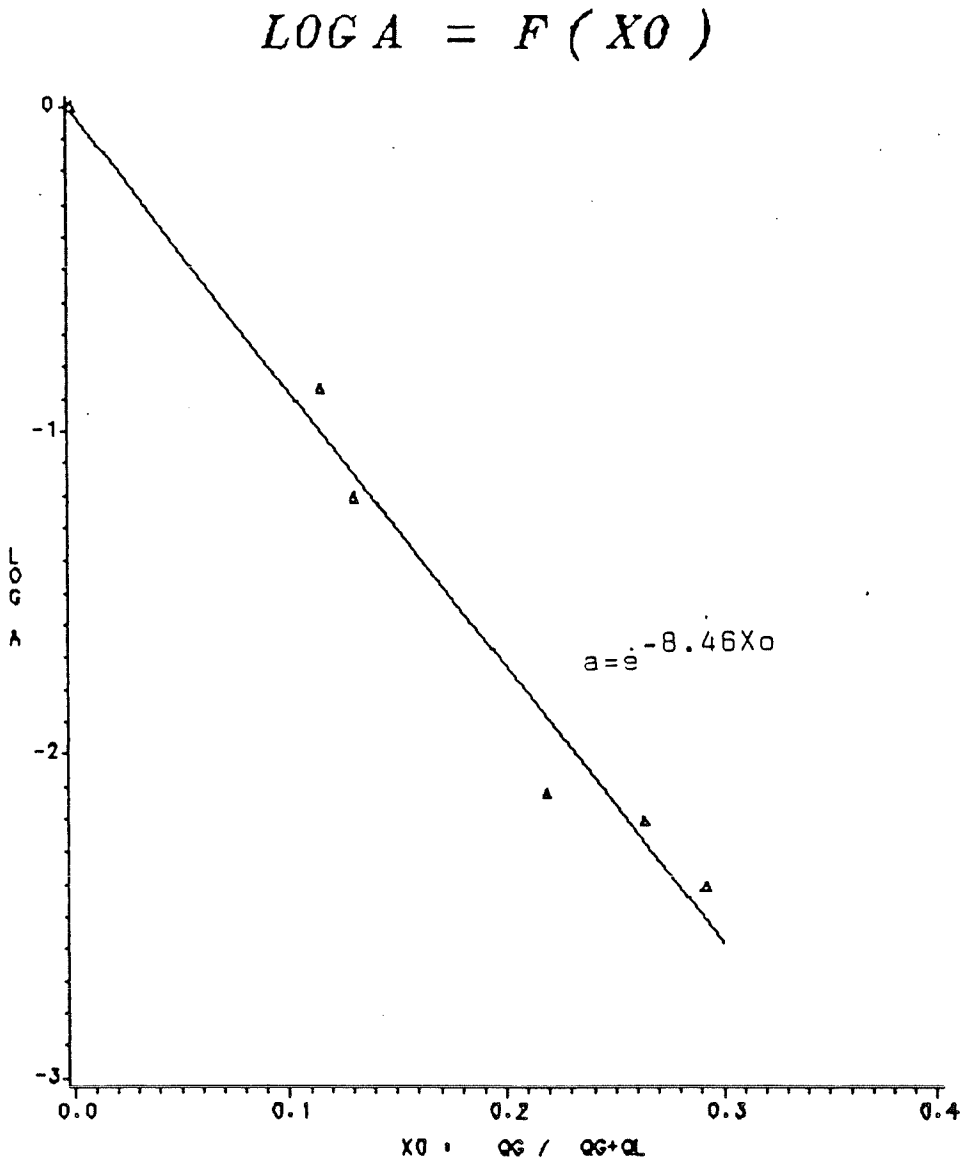

FIGURE 23:

Variation of exponent "a" in power & exponential model of void fraction in terms of flow volumetric quality X_o.

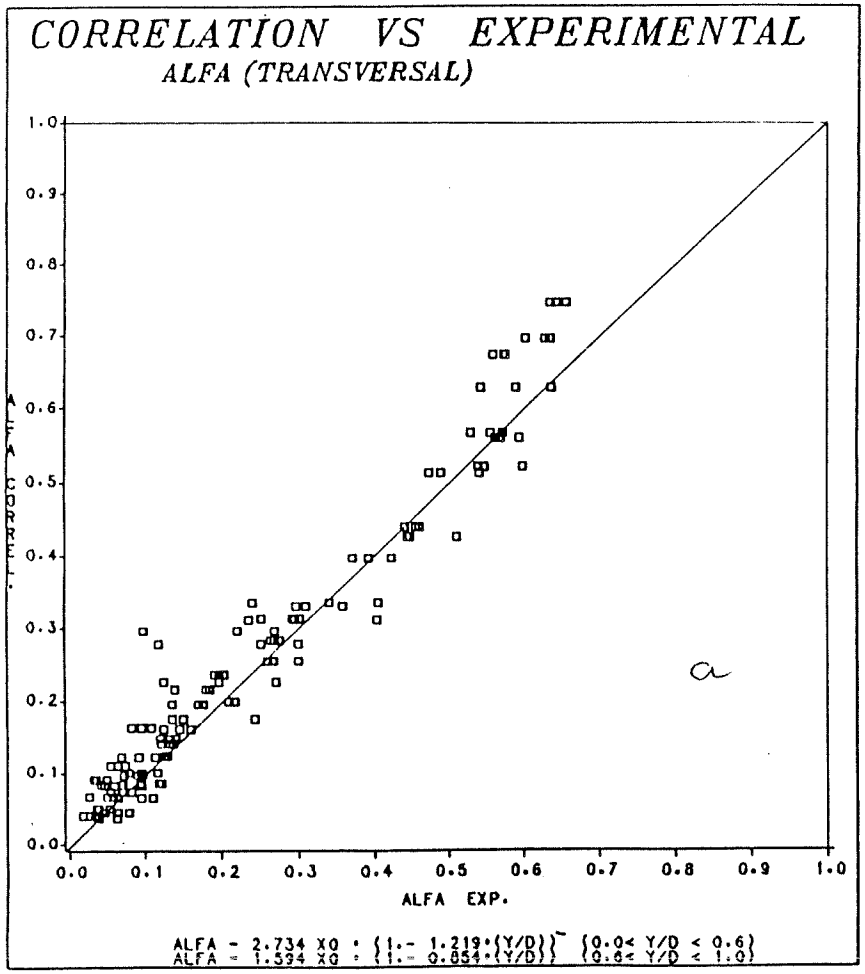

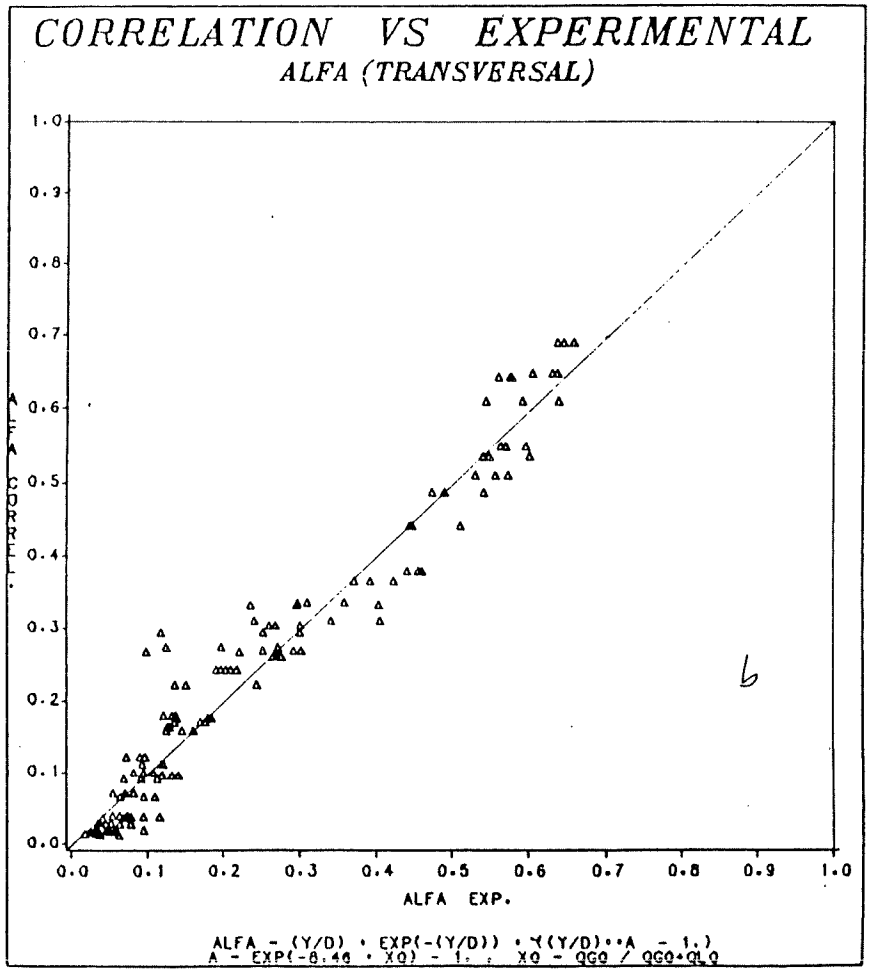

FIGURE 24: Comparison between experimental results and proposed void correlations in transversal plane

(a: linear model, b: power & exponential model)

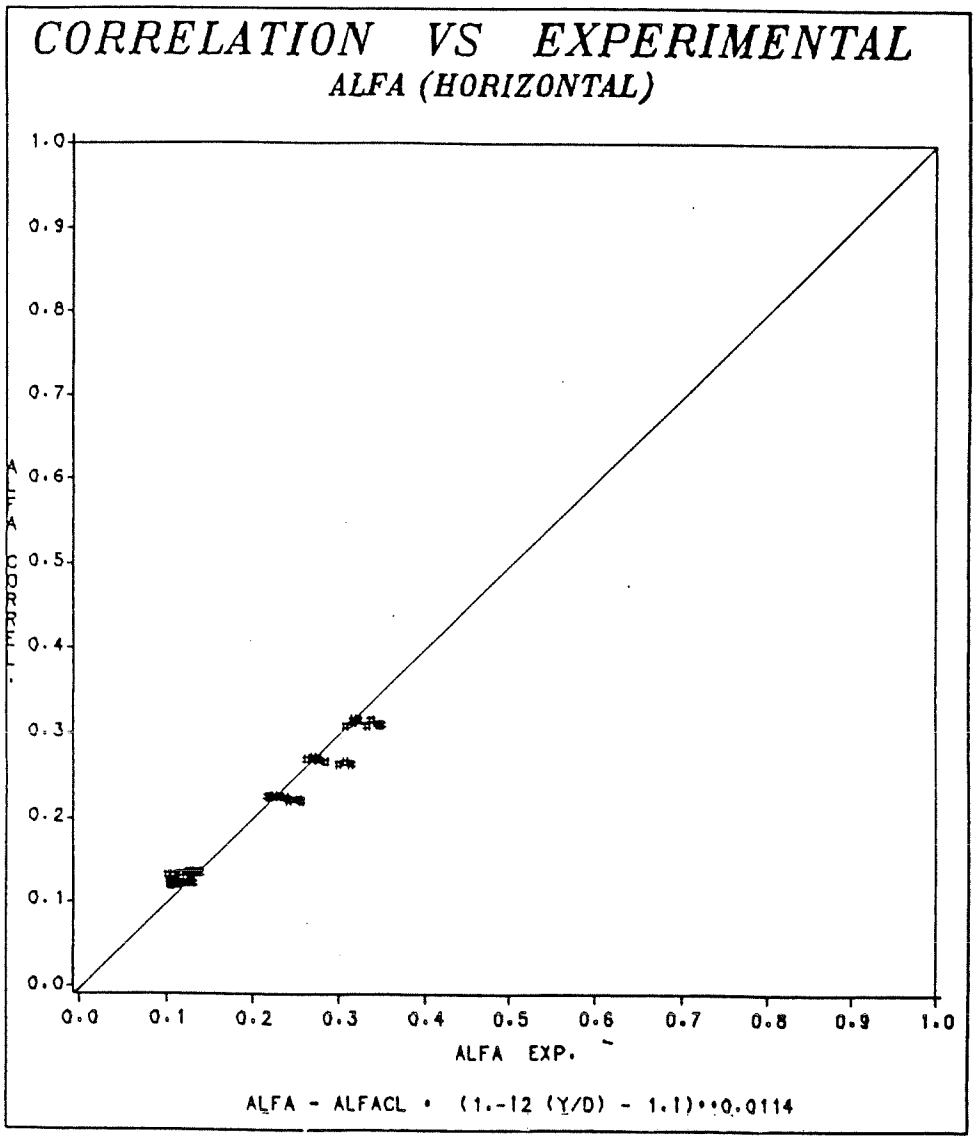

FIGURE 25:

Comparison between experimental results and proposed void correlations in radial plane